

THE UNIVERSITY OF CALGARY

APPLICATION OF
STRAPDOWN INERTIAL SYSTEMS
FOR PRECISE PIPELINE MONITORING

by:

Todd Russel Porter

A DISSERTATION
SUBMITTED TO THE FACULTY OF GRADUATE STUDIES
IN PARTIAL FULFILLMENT OF THE REQUIREMENTS FOR THE
DEGREE OF

Master of Engineering

DEPARTMENT OF SURVEYING ENGINEERING

CALGARY, ALBERTA

AUGUST, 1990

© Todd Russel Porter, 1990



National Library
of Canada

Acquisitions and
Bibliographic Services Branch

395 Wellington Street
Ottawa, Ontario
K1A 0N4

Bibliothèque nationale
du Canada

Direction des acquisitions et
des services bibliographiques

395, rue Wellington
Ottawa (Ontario)
K1A 0N4

Your file *Votre référence*

Our file *Notre référence*

The author has granted an irrevocable non-exclusive licence allowing the National Library of Canada to reproduce, loan, distribute or sell copies of his/her thesis by any means and in any form or format, making this thesis available to interested persons.

L'auteur a accordé une licence irrévocable et non exclusive permettant à la Bibliothèque nationale du Canada de reproduire, prêter, distribuer ou vendre des copies de sa thèse de quelque manière et sous quelque forme que ce soit pour mettre des exemplaires de cette thèse à la disposition des personnes intéressées.

The author retains ownership of the copyright in his/her thesis. Neither the thesis nor substantial extracts from it may be printed or otherwise reproduced without his/her permission.

L'auteur conserve la propriété du droit d'auteur qui protège sa thèse. Ni la thèse ni des extraits substantiels de celle-ci ne doivent être imprimés ou autrement reproduits sans son autorisation.

ISBN 0-315-79224-8

Canada 

**THE UNIVERSITY OF CALGARY
FACULTY OF GRADUATE STUDIES**

The undersigned certify that they have read, and recommend to the Faculty of Graduate Studies for acceptance, a thesis entitled, "Application of Strapdown Inertial Systems for Precise Pipeline Monitoring" submitted by Todd Russel Porter in partial fulfillment of the requirements for the degree of Master of Engineering.

K.P. Schwarz

Supervisor, Dr. K.P. Schwarz
Department of Surveying Engineering

G. Lachapelle

Dr. G. Lachapelle
Department of Surveying Engineering

W.F. Teskey

Dr. W.F. Teskey
Department of Surveying Engineering

H.A.R. de Paiva

Dr. H.A.R. de Paiva
Department of Civil Engineering

J.R. Adams

Mr. J.R. Adams
President, Pulsesearch Consolidated Technology Ltd.

DATE

Aug. 31, 1990

ABSTRACT

A unique application of strapdown inertial technology has been developed for deformation monitoring of operating pipelines. The instrumented system called a Geometry Pig determines position, orientation, curvature, ovality, and deformations such as dents and wrinkles of oil and gas pipelines. At the heart of this integrated system is a Strapdown Inertial Navigation System which is integrated with velocity and distance sensors, caliper sensors, weld detection system, and digital recording device. The geometry pig is designed to operate continuously and autonomously in operating fluid or gas pipelines. The study presents the motivation, design concepts, system description, mathematical models for processing inertial and other sensor data, and an analysis of the capabilities. Results from operating oil pipelines are presented which demonstrate the accuracies obtained meet or exceed the requirements for pipeline geometry monitoring.

ACKNOWLEDGEMENTS

The author would like to thank his supervisor, Dr. Klaus-Peter Schwarz, for his input and accessibility throughout the research, preparation and completion of this document. Special thanks are given to the people of Pulsesearch Consolidated Technology Ltd., Calgary, Alberta for this opportunity, in particular Mr. John Adams who shared his broad knowledge of inertial navigation, and Mr. James Smith who continually stressed the importance of the raw observable. The critique by Dr. Ernst Knickmeyer, also from Pulsesearch, is greatly appreciated.

The author wishes to acknowledge Interprovincial Pipeline Company (IPL), Edmonton, Alberta, for their confidence and support in this new technology developed at Pulsesearch. All data presented in this report is courtesy of IPL.

*To my wife, Sheridan
for her support and encouragement*

NOTATION

All matrices throughout the document are denoted in bold upper case letters (eg. \mathbf{A}), vectors are annotated in lower case with the vector symbol (eg. \vec{v}), and scalar quantities may be lower or upper case with normal attributes. A transformation matrix such as \mathbf{R}_b^n , performs a rotation from the "b" frame to the "n" frame. Similarly, a value such as $\vec{\omega}_{ib}^n$, denotes the angular rate of the "b" frame relative to the "i" frame coordinatized in the "n" frame. This convention, complete with examples, is detailed in (Britting, 1971).

ϕ	geodetic latitude, or roll angle
λ	geodetic longitude
h	ellipsoidal height
Θ	pitch angle
ψ	yaw angle
κ	curvature
i	inertial frame (super/sub script)
p	sensor block frame (super/sub script)
b	body frame (super/sub script)
e	earth frame (super/sub script)
n	local level frame (super/sub script)
\vec{f}	specific force
\vec{a}	acceleration
\vec{v}	velocity
\vec{r}	position
\mathbf{R}_j^i	matrix to rotate quantities from system "j" to system "i"
$\vec{\omega}_{ij}^k$	angular velocity of the "j" system with respect to the "i" system, coordinatized in the "k" system
$\vec{\Omega}_{ij}^k$	skew symmetric matrix of $\vec{\omega}_{ij}^k$
ω_e	earth rate (rad/sec)

a	ellipse semi-major axis
b	ellipse semi-minor axis
e	ellipse eccentricity
ω	$= (\omega_e + \dot{\lambda})$
$\Delta\vec{\Theta}$	angular increments
$\Delta\vec{v}$	velocity increments
R_N	prime vertical radius
R_M	meridian radius
R_E	$= R_N \cos \phi$ (latitude)
Φ	transition matrix
F	dynamics matrix
K	gain matrix
C_i	covariance matrix of "i" parameters
\dot{x}	time derivative
\hat{x}	estimated quantity
(-)	quantities before update
(+)	quantities after update

Table of Contents

1 INTRODUCTION	1
1.1 Problem Definition	1
1.2 Inertial Measurement Units	2
1.3 Design Considerations	3
1.4 Organization of Dissertation	6
2 INTEGRATED SYSTEM DESCRIPTION	7
2.1 Strapdown Inertial Navigation System (INS)	7
2.1.1 Gyroscopes	8
2.1.2 Accelerometers	10
2.1.3 Digital Pulse Interface	11
2.2 Caliper Sonar	13
2.3 Chainage and Velocity	16
2.4 Weld Detect	17
3 MATHEMATICAL MODELS	19
3.1 Overview of Modelling Tasks	19
3.2 Reference Frames	20
3.3 Calibration / Alignment	23
3.4 Navigation / Mechanization	27
3.4.1 Compensation	28
3.4.2 Accelerometer Stream	30
3.4.3 Gyro Stream	33
3.5 Kalman Filter	38
3.5.1 Introduction	38
3.5.2 Velocity Updates	44
3.6 Curvature	47
3.7 Computational Considerations	51
4 PIPELINE MONITORING RESULTS	54
4.1 Single Run Analysis	54
4.1.1 Alignment Analysis	54
4.1.2 Kalman Filter Parameters	61
4.1.3 Results	62
4.2 Multiple Run Deformation Analysis	67
4.2.1 Results	67
5 SUMMARY & CONCLUSIONS	74
6 BIBLIOGRAPHY	76

Table of Tables

Table 2-1. Digital Output Signals	13
Table 3-1. Direction Cosine vs. Quaternion	34
Table 4-1. Gyro Drift Estimation Results	55
Table 4-2. Accelerometer Bias Estimation Results	55
Table 4-3. Alignment Orientation Results	56
Table 4-4. Kalman Filter Initialization Parameters	61
Table 4-5. Fine Alignment Orientation Results	62

Table of Figures

Figure 1-1. Pig Train for Small Diameter Pipelines	4
Figure 1-2. Single Carrier Pig for Large Diameter Pipelines	5
Figure 2-1. Integrated System Structure	7
Figure 2-2. Classification of Gyroscopes	8
Figure 2-3. Single Degree of Freedom Gyro Mechanism	9
Figure 2-4. SDF Gyro Impulse and Momentum	10
Figure 2-5. Electrostatic Force Rebalance Pendulous Accel	11
Figure 2-6. Honeywell H778 Functional Block Diagram	12
Figure 2-7. Caliper Sonar Adjustment	13
Figure 2-8. Odometer Sensors	17
Figure 3-1. Local Level Strapdown Mechanization	20
Figure 3-2a. Inertial Reference Frame	21
Figure 3-2b. Earth Frame	21
Figure 3-2c. Local Level Frame	22
Figure 3-2d. Sensor Block Frame	22
Figure 3-2e. Body Frame	23
Figure 3-3. Pipeline Curvature	48
Figure 3-4. Effect of Data Rates on Attitude	52
Figure 3-5. Effect of Quantization on Attitude	53
Figure 3-6. Effect of Commutativity on Attitude	53
Figure 4-1a. Alignment Velocity Errors - Run 1	58
Figure 4-1b. Alignment Position Errors - Run 1	58
Figure 4-2a. Alignment Velocity Errors - Run 2	59
Figure 4-2b. Alignment Position Errors - Run 2	59
Figure 4-3a. Alignment Velocity Errors - Run 3	60
Figure 4-3b. Alignment Position Errors - Run 3	60
Figure 4-4. Raw H778 Output	64
Figure 4-5. Navigation Results	65
Figure 4-6. Caliper Results	66
Figure 4-7. Longitude Errors	69
Figure 4-8. Latitude Errors	69
Figure 4-9. Height Errors	70
Figure 4-10. Vertical Curvature - Run 1	71
Figure 4-11. Vertical Curvature Comparison	71
Figure 4-12. Horizontal Curvature - Run 1	72
Figure 4-13. Horizontal Curvature Comparison	73

1 INTRODUCTION

1.1 Problem Definition

The focus of this research is the application of strapdown Inertial Navigation Systems (INS) for deformation monitoring of pipelines. The major objective of deformation monitoring is to collect the information to allow analysis that will prevent structural failure of the line caused by deformation. Deformations and physical damage are typically caused by external forces such as: earthquakes, landslips, subsidence and floods, and often third party damage resulting from encroachment. The consequences of failure of the line may be serious, both for the environment and financially for the operator of the pipeline.

The inspection of a pipe has to accomplish two tasks. Critical deformations have to be detected and also located. A pipe can be buried, underwater, hanging from bridges, passing tunnels etc. so that classical surveying methods (from the outside) are not appropriate. The pipe must be measured directly, accurately, and at high resolution to ensure that no anomalies are missed. With the availability of strapdown units which are inexpensive, small, suitably accurate, and which require low power for operation, deformation monitoring of operating pipelines is possible.

The use of an autonomous navigation system such as a strapdown INS to survey a pipeline from the inside out provides a solution for measuring pipeline geometry. Position and curvature of the centre line are computed from measurements given by the strapdown INS, with other sensors providing location by measuring chainage. Additional geometric quantities such as ovality, dents, and features such as circumferential welds, valves, and changes in pipe wall thickness are computed from measurements of other sensors on the system. A complete geometry database for the pipeline at very high resolution is generated.

The sensors are contained in a so called "pig". The name arose from early versions of devices which travelled through operating pipelines pushed by the fluid or gas to scrape and clean the pipe walls. They made a squealing noise during operation, hence appropriately named "pig". All devices which work internally on a pipeline are described as pigs. An extensive list of current pigs and technology is provided in (Palmer and Jee, 1990), which classifies pigs for: separation of products, cleaning out deposits and debris, gauging the internal bore, location of obstructions, meter loop calibration, liquids removal, gas removal, **pipe geometry measurements**, internal inspection, coating of internal bore, corrosion inhibition,

improving flow efficiency, stopping flow, detection of metal loss, and locating and measuring cracks and flaws. Pipeline geometry determination is therefore only one possible task of a pipeline pig.

1.2 Inertial Measurement Units

During the past two decades, Inertial Navigation Systems (INS) have been used as an effective survey tool for a wide variety of applications. These applications include navigation and positioning for gravity surveys, mapping of resources, topography, transportation and utility corridors, inventory surveys, and oil and gas exploration surveys. Various modes of transport by airborne, land, and rail vehicles have proven the economic benefit and demonstrated accuracies and production rates which by other conventional methods of survey could not be realized.

Typically, inertial navigation systems used have been of the stable platform type. Stable platform INS have serious shortcomings, however, in that;

- for survey applications they are large, thereby excluding certain applications
- they are mechanically complex, and consequently have a higher failure rate
- they require significant power to operate
- they require real time computing power
- they are expensive to purchase and to maintain
- they are limited in dynamic response.

Strapdown INS are characterized by the direct attachment of the inertial sensors to the body of the INS unit. No mechanism, such as gimbals, are used for isolating vehicle motion, so the total motion of the INS body frame is sensed. In the past, strapdown sensors have not performed well in dynamically extreme environments. Recent developments in strapdown sensor technology have to a great extent overcome these problems, and opened up numerous applications of this technology.

Strapdown systems differ from the stable platform INS by the following,

- they are much smaller because of the elimination of gimbals, and related hardware
- they require less power
- they require little real-time computing power; data can be logged for subsequent analysis

off-line.

- they are cheaper to manufacture
- their measurement range is larger

For reasons discussed in §1.3, the Honeywell H778 was the system selected for use in the geometry pig. This system is classified as low accuracy. It comes as a sensor unit and can be used in a variety of applications by interfacing to an external computer and using the proper software for guidance, control, or navigation. Some of the applications that use the H778 are; tactical missile midcourse guidance, sensor stabilization and control, torpedoes, torpedo targets, and undersea research vehicles, manned and unmanned aircraft, drones, decoys, and special instrumentation.

The advantage of using a strapdown unit is that the software algorithms can be designed specifically for the mission requirements which may call for different levels of accuracy, order, or speed. For example, the requirements of the pig vary drastically from most of the above in that there is no real time computing and guidance requirement, and the operating environment of the pipeline is benign in comparison to other applications.

1.3 Design Considerations

The geometry pig was designed in modular form to service a large variety of pipelines. Criteria for size of components, power requirements, reliability, accuracy, and operating ranges limited the choice of available components to construct the instrument. Operating scenarios for oil or gas lines called for a system capable of measuring accurately, and continuously in a line. Line diameters vary from Nominal Pipe Size 12 inch diameter (NPS-12), up to NPS-56 inch diameter. The pig design is modular allowing for configuration and component changes to adapt to a particular pipeline and survey requirement. This allows for the use of different strapdown systems in the pigs.

Due to the nature of inertial measurements regular "updates" of attitude, position, and velocity are required to control system errors. External position and attitude may be taken from pipeline "as built" plans for surface identifiable pipeline features such as valves, and launch/receive trap facilities. Zero velocity UPdaTeS (ZUPTS) are not possible when the pig is travelling along with the oil or gas in the operating pipeline. Thus velocity sensors are used to provide velocity with respect to the pipeline wall for updates. Odometers are mounted on the tail of each pig, as shown in Figure 1-1 and Figure 1-2, which measure the

distance travelled and velocity. The location of any detected geometric anomaly is required to within 10m. This is achieved by combining the chainage and positioning accuracy of the pig system with coordinated features.

The requirement for curvature accuracy calls for measurement of pipeline radius of curvature to 100m over a 2m section of pipe. A low accuracy system such as the Honeywell H778 is capable of delivering this accuracy for curvature measurement. The gyro drifts of the H778 are $10^\circ/\text{hr}$, suitable for the curvature requirement. This accuracy along with size, power requirements, and reliability were the basis for selection of this system.

The instrumentation including the strapdown INS, are housed in sealed pressure canisters called carriers (see Figure 1-1 and 1-2). Each carrier is suspended in the pipeline by rubber suspension disks at front and aft of each carrier. This guides the pig to move close to the pipe centre line. However, this guidance is not accurate enough to assume that the trajectory (position) of the pig coincides with the pipe centre line, and that the pig's pitch and heading coincide with that of the pipeline. The actual deviations have to be determined continuously. This is achieved by two rings of caliper sonars mounted close to the suspension disks. In Figure 1-1, the canister labelled "inertial" houses the sonar devices, whereas Figure 1-2 shows the sonars mounted behind each double set of suspension rubbers. They measure the distance to the wall of the pipeline and yield the pig-to-pipe translation and attitude corrections for pipe centreline coordinates and pitch and heading of the pipe. Simultaneously a complete picture of the inner shape of the pipeline is generated. Here the information for dents and ovality to an accuracy of 1mm as well as feature identification of valves, wall thickness changes, etc. is extracted.

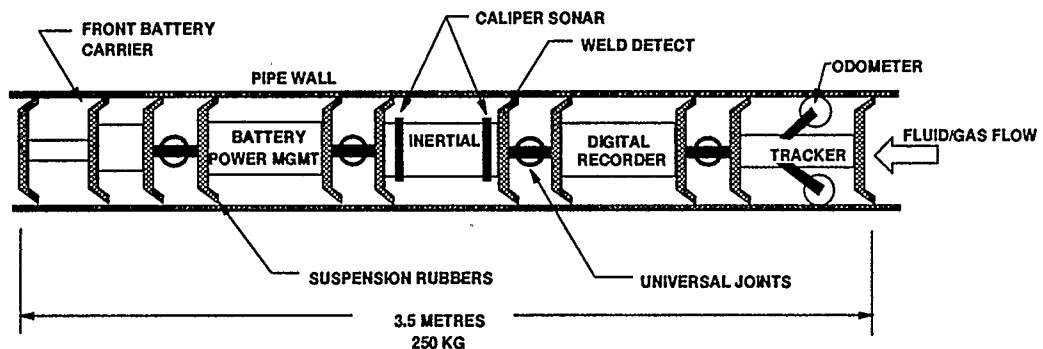


Figure 1-1. Pig Train for Small Diameter Pipelines

Pressure and temperature sensors determine operating conditions of the pipeline. A tracking transmitter is contained in the last canister of the pig (Figure 1-1), or attached on the end of the single carrier as in Figure 1-2 for monitoring location of the pig during its run. This instrument is a requirement of all pipeline operators.

The detection and determination of deformations occurring between runs at different time epochs require the precise correlation of pipeline features. The method to achieve this match is based on the identification of circumferential welds which occur approximately every 10-20m.

The storage device and related electronics fill another canister for the small diameter tool Figure 1-1 whereas in Figure 1-2 they make up another module in the single carrier. The batteries provide power for the sensors, recording device and on-board computers used to manage the data.

The pig must be able to safely pass through 3D radius bends (3 times the pipe diameter). The strapdown INS and recording device limited the smallest diameter to NPS-12, as shown in the multi-carrier version in Figure 1-1. A single carrier version of the pig designed for diameters larger than NPS-22, is shown in Figure 1-2, which again safely passes through 3D radius bends in the pipeline.

A detailed description of trade-offs and considerations which led to the geometry pig is given in (Adams et al, 1989).

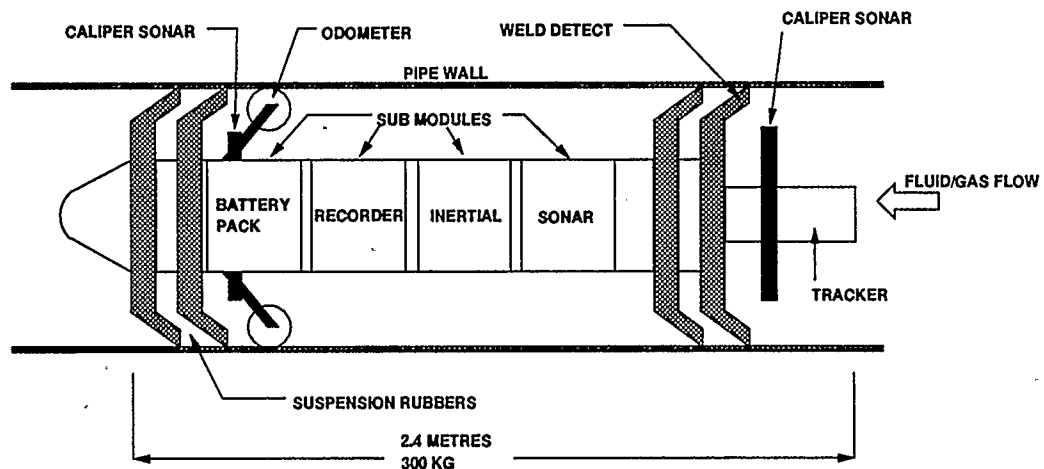


Figure 1-2. Single Carrier Pig for Large Diameter Pipelines

1.4 Organization of Dissertation

The major sections to follow are subdivided into Integrated System Description, Mathematical Models, Pipeline Monitoring Results, and Summary & Conclusions.

In the next section, Integrated System Description, a review of the design of the geometry pig is given. Major sensor components are presented such as; the strapdown INS, caliper sonar system, velocity sensors, and weld detect. Each component is detailed and functionality described with respect to the overall system.

Section three, Mathematical Models, presents the models used to process the sensor information. The strapdown INS models for calibration/alignment, mechanization, and Kalman filtering are given. This is followed by discussing how to obtain curvature and some computational considerations unique to this application.

Section four, Pipeline Monitoring Results, presents the outcome from projects carried out on operating pipelines. Single and multiple run analyses are given and results are discussed.

The final section summarizes the advantages, results and accuracy, benefits and applications of this system.

A project of this nature involved specialists in the areas of electrical, mechanical, surveying, and structural engineering as well as machinists, and systems analysts. The author was involved primarily in the mathematical modelling, software development, and analysis of data for the pipeline geometry pig. He also participated in prototype testing in the field and designed calibration procedures for the sensors.

2 INTEGRATED SYSTEM DESCRIPTION

The integrated hardware design is comprised of the strapdown INS (primary sensor), and odometer wheels, caliper sonar transducers, weld detectors which make up the additional sensor group. The data of these additional sensor measurements are processed for further use as updates and pig-to-pipe transformations, or final geometric quantities directly. Support components are power and power management modules, a small PC computer to manage the sensor data, and a digital tape recording system for storage. These sensors and their processing modules are described in the following sub-sections. The functional block diagram of the integrated system is shown in Figure 2-1.

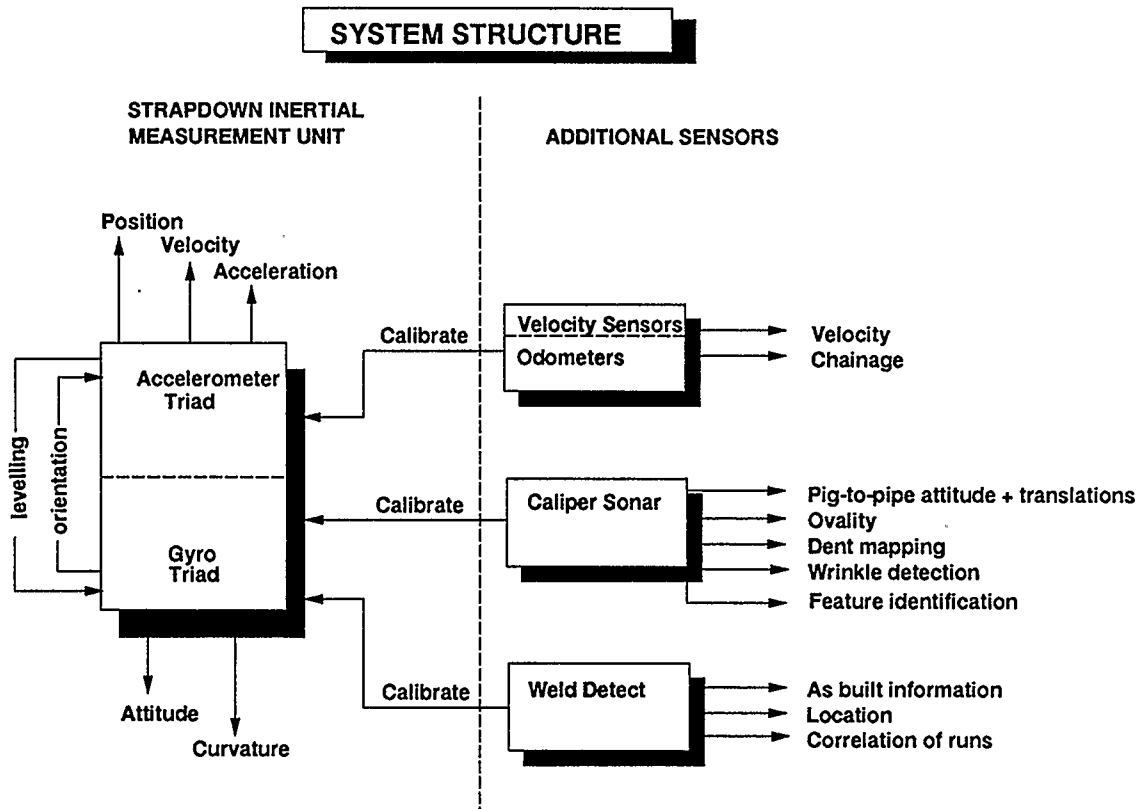


Figure 2-1. Integrated System Structure

2.1 Strapdown Inertial Navigation System (INS)

The strapdown inertial system is the heart of the geometry pig. It produces 3-dimensional measurement of specific force and angular rate of the sensor assembly directly from orthogonal triads of accelerometers and single degree of freedom gyros. The accelerometers

and gyros are complementary sensors which, when coupled, present a dead-reckoning navigation instrument. It delivers the measurements for computing pipeline curvature and the positioning of all detected features.

2.1.1 Gyroscopes

The numerous gyro designs which have been manufactured or proposed can be conveniently subdivided into rotor and non-rotor designs as shown in Figure 2-2.

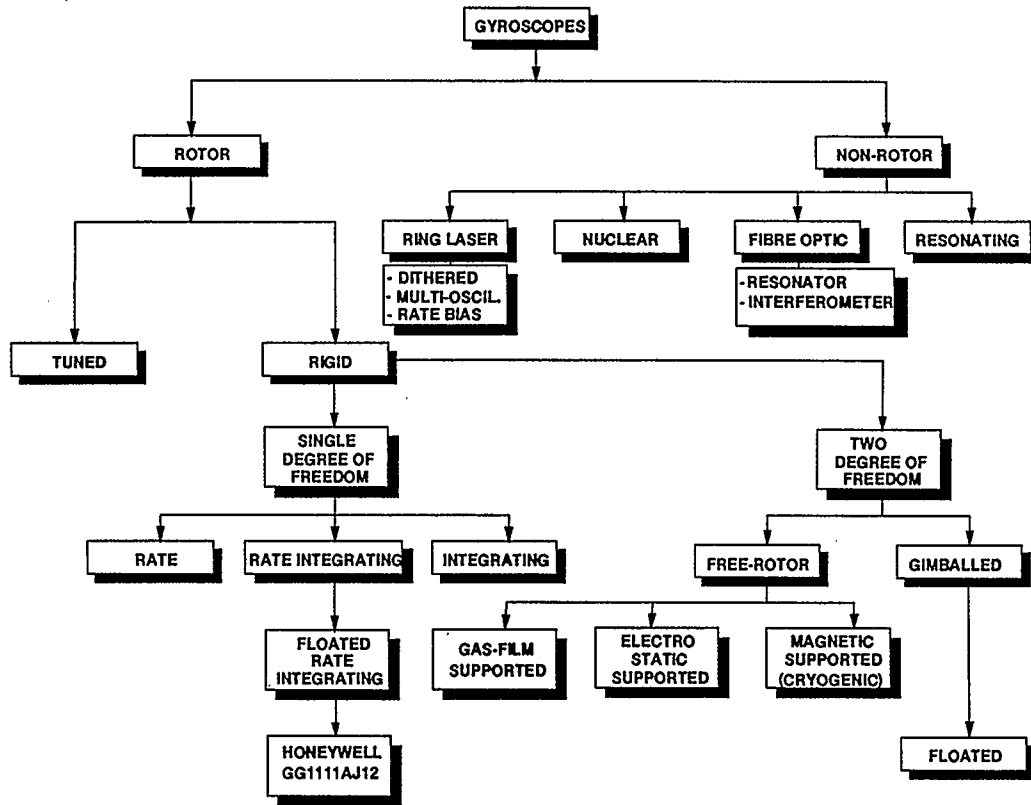


Figure 2-2. Classification of Gyroscopes by Rotor and Suspension Design
(Rüeger, 1982, with modifications)

These sensors provide precision measurements of the strapdown sensor "body frame" angular rotation rate relative to non-rotating inertial space. The discussion of gyroscopes will be restricted to sensors used in strapdown platforms, more specifically, the gyros used in the H778 strapdown INS. The H778 contains single degree of freedom (SDF), floated rate-integrating gyros (FRIG) mounted in an orthogonal triad to provide 3-dimensional angular rate measurement.

The principal components of the SDF-FRIG are depicted in Figure 2-3. The three axes of the sensor are; spin axis (X), input axis (Y), and output axis (Z). The float (or gimbal) provides the one degree of freedom (discounting the spin axis) of the gyro, thus it is sensitive in only one direction. The measurement principle is based on the relationship between the input axis and the resultant $\Delta\phi$ about the output axis. This relationship is defined by examining the total angular momentum of the gyro system.

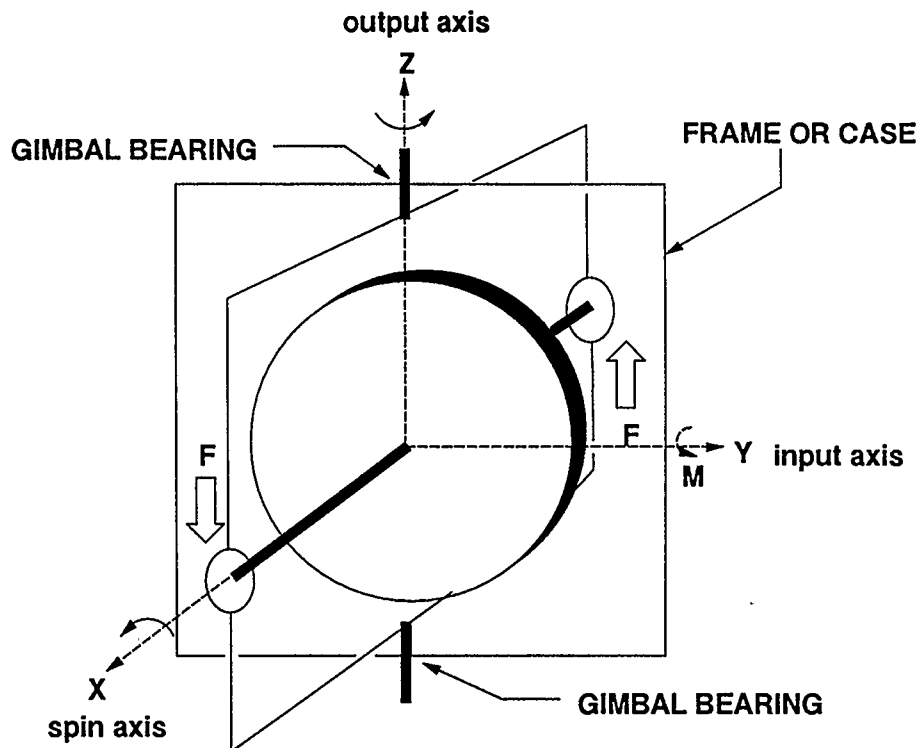


Figure 2-3. Single Degree of Freedom Gyro Mechanism

In order to understand how an angular change is measured by the gyro, some basics of the behavior of mechanical gyros are introduced. An undisturbed spinning mass gyro is shown in Figure 2-4a, where I_g = spinning mass moment of inertia, and ω = rotation rate of the gyro about the X axis (spin axis). The direction of the spin axis in inertial space is fixed as long as the angular momentum $I_g\omega$ is constant. When a torque $M\Delta t$ is imposed on the gyro as shown in Figure 2-4b about the Y axis (input axis), the angular momentum is changed and the gyro starts to precess about the Z axis (output axis) by $\Delta\phi$ as shown in Figure 2-4c. Since *the rate of increase of angular momentum about a point equals the input torque about that point* (Beer and Johnson, 1976) the change in the direction of the spin axis can be

measured. This relates the applied torques to the measured output axis deflection angle $\Delta\phi$. The output of the rate gyro is obtained by measuring the rotation of the gimbal about the output axis.

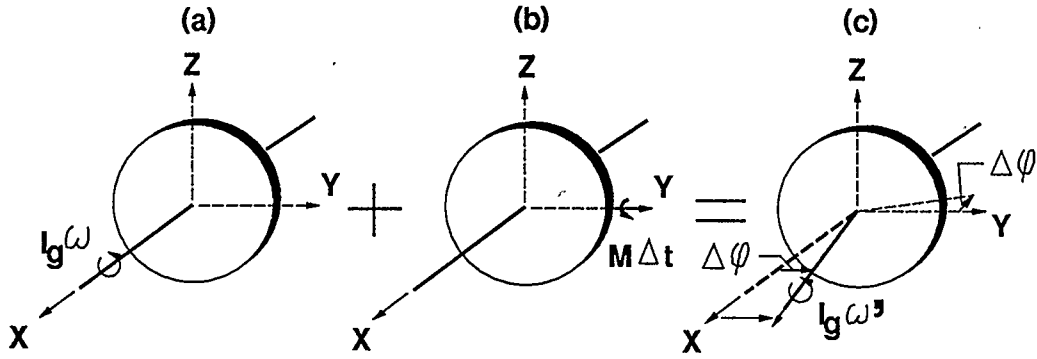


Figure 2-4. SDF Gyro Impulse and Momentum

To complete the description of the SDF-FRIG, the rate integrating method of angular measurement is performed by limiting the output gimbal motion to a few degrees. This is done by closed loop gimbal torquing to maintain the deflection near null. Near frictionless gimbals support the gyro, and no spring restraints are required to damp gimbal angular excursions. The real time accuracy of these gyros is high due to the fact that the gyro excursions are minimal in dynamic response to input rotations. The output is the required torque current to maintain the frictionless and unrestrained gimbal at or near the null position.

2.1.2 Accelerometers

Accelerometers provide measurements of specific force along a sensitive axis. The basic measurement principle used in accelerometers is the detection of movement of a proof mass, or electrode as shown in Figure 2-5. In open loop systems, the deflection or the translation of the proof mass is measured, whereas closed loop systems provide feedback in order to control the movement of the proof mass or balance it to some null or zero position. Accelerometers may be classified according to;

- geometry of path of the proof mass,
- the number of degrees of freedom of the proof mass,
- the method of suspension of the proof mass,
- the output quantity of the accelerometer,
- the type of constraint of the proof mass.

Detailed descriptions of these classes may be found in (Rüeger, 1986). The most common type of accelerometer used today is the closed loop force rebalance system of either pendulous or translational type. They are used in the H778 and are of the Q-Flex closed loop pendulous force rebalance variety. Figure 2-5 depicts the components of these sensors and the feedback mechanism for balancing the pendulous proof mass which is suspended by quartz flexure elements to the case.

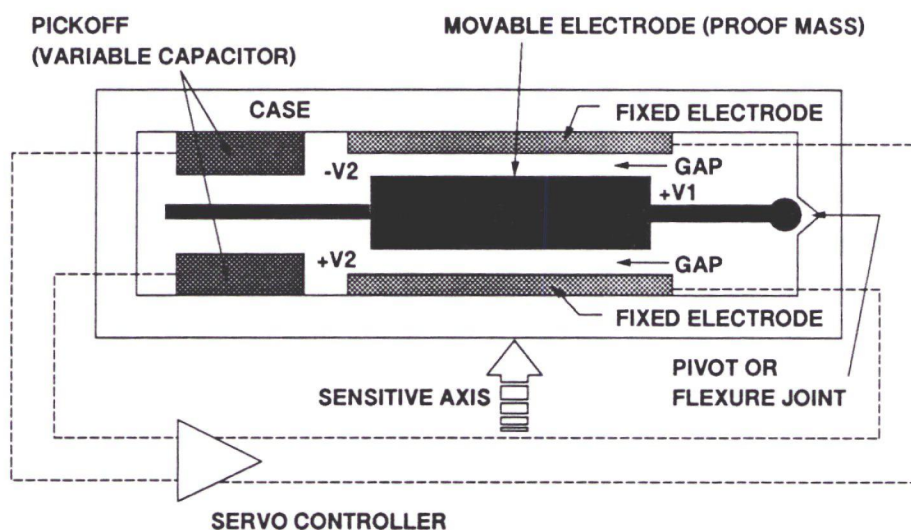


Figure 2-5. Electrostatic Force Rebalance Pendulous Accelerometer (Rüeger, 1986)

The balancing forces required to maintain the air gaps and null position are provided by an electrostatic force which is a function of the electrode potentials (V). Electrostatic accelerometers such as the Q-Flex class have the advantages of mechanical simplicity, low power requirements, capability of producing large rebalance forces (thus high dynamic range), no hysteresis errors, and zero temperature coefficient. These factors are very much suited to strapdown configurations.

2.1.3 Digital Pulse Interface

Input motion of the strapdown INS, accelerations and angular rates, are sensed by the accelerometers and gyros as described. These signals are sent to the loop electronics for generation of drive signals which are sent back to balance the accelerometer pendulum or gyro gimbal to null. This sensed input motion provides input to the integrators for further processing or, at this point, output in analog format.

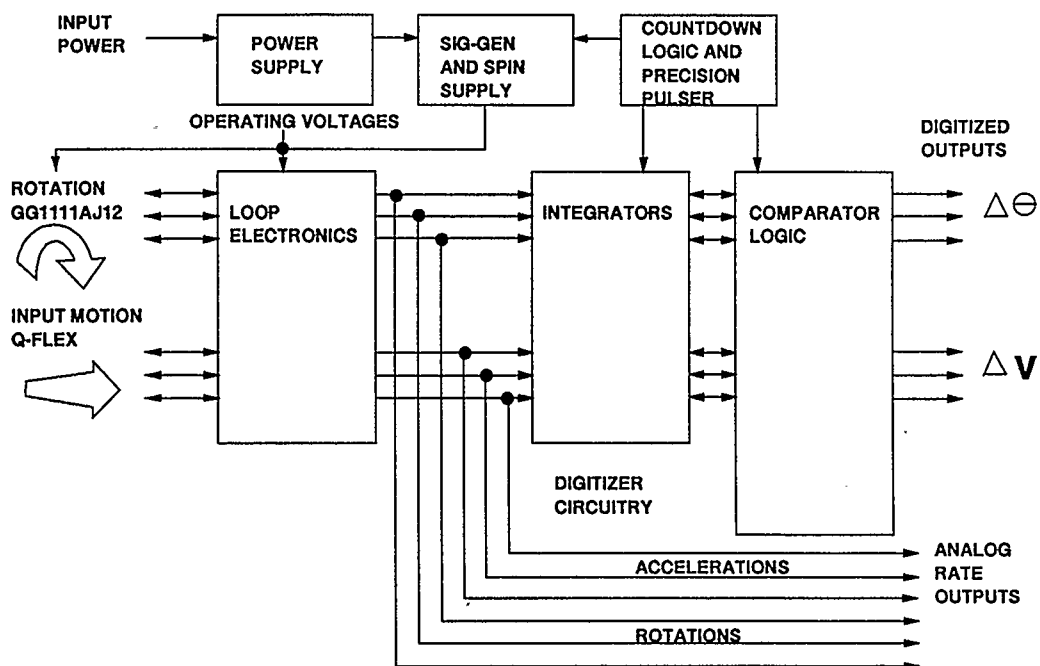


Figure 2-6. Honeywell H778 Functional Block Diagram

As shown in Figure 2-6, reference and timing signals are also inputs to the digitizer circuits. The precision pulse generator provides a continuous pulse train that is used as reference, and the timing generator supplies the precision timing pulses used by both the precision pulse generator and the digitizer circuitry. A crystal controlled oscillator provides the stable frequencies used by the digitizer circuitry.

The digitizer circuitry, integrators, and comparator logic provide digitized output pulses as a function of the time-integral of the analog loop output voltages. The digitizer circuitry outputs are in the form of $\Delta\bar{\theta}$ (incremental changes in attitude) and $\Delta\bar{v}$ (incremental changes in velocity). The signal generator and spin supply provides power to all three gyro spin motors and power for the gyro signal generators (Honeywell, 1985). The incremental outputs are in the form of pulses, the pulse having a corresponding weight factor assigned in order to convert to physical units of velocity and angular increments (see Table 2-1). The method of digitizing the analog voltages is by means of quantization.

Table 2-1. Digital Output Signals

Output Signal	Pulse Weight	Max. Pulse Rate	Range
$\Delta\theta$	25.1787 "/pulse	12.8 kHz	88 °/s
Δv	0.0047625 m/s/pulse	12.8 kHz	15 g

2.2 Caliper Sonar

The sonar ring measures distances from the pig carrier to the pipe wall, thus capturing a cross section of the pipe. These ranges are processed using adjustment techniques to compute the centre of the pipe with respect to the pig and the pig-to-pipe attitude using circular and ellipsoidal models. Deviations from the model (adjustment residuals) give the cross sectional picture of the pipe with determination of dents and ovality as shown in Figure 2-7.

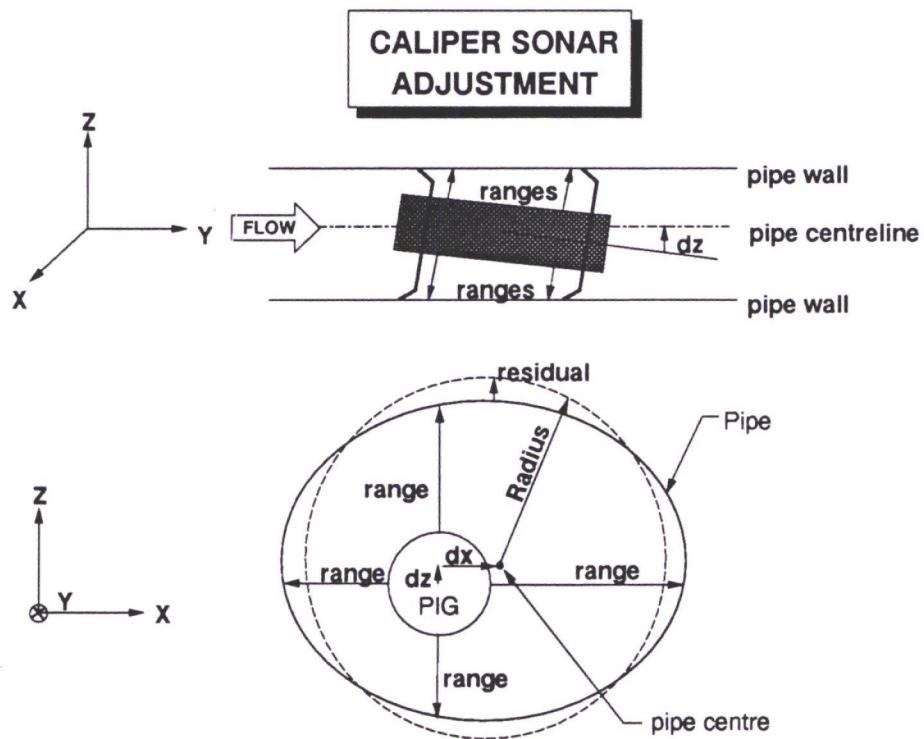


Figure 2-7. Caliper Sonar Adjustment

Valve locations, tee junctions, and heavy/thin wall sections are identified and may be used as control points if as-built information is available. This provides direct cross reference between the measured geometry and as-built information. Statistical measures of the accuracy are provided with the computed covariance matrix for the unknowns.

The sonar devices are mounted in a ring and spaced at precisely machined constant angles around the ring on the pig (Figure 1-1 and Figure 1-2). An accurate offset is added to these ranges to give the actual distance from the centre of the carrier to the pipe wall. These observations are in a polar coordinate system (r, Θ) and are converted to a rectangular coordinate system (x, z) to form the pseudo-observations. The models are translated-circle and translated-rotated-ellipse written for observations in a rectangular system.

The circle model is,

$$f(x, l) = (x + d_x)^2 + (z + d_z)^2 - R^2 = 0 \quad (2-1)$$

The ellipse model is,

$$f(x, l) = \frac{(x \cos \alpha + d_x)^2}{a^2} + \frac{(z \sin \alpha + d_z)^2}{b^2} - 1 = 0 \quad (2-2)$$

where; $f(x, l)$ functional dependency of unknowns and observations respectively

α orientation of the ellipse axes

d_x, d_z translation components

R circle radius

a, b ellipse semi-major, semi-minor axes

The formulation of the least squares problem is represented by the differential form of the original system of non-linear equations given above.

$$\vec{A}\vec{\delta} + \vec{B}\vec{r} + \vec{w} = 0 \quad (2-3)$$

where; $\vec{A} = \frac{\partial f}{\partial x} \Big|_{x=x^{(0)}, l=l^{(0)}}$

$\vec{\delta}$ = unknowns

$$\mathbf{B} = \frac{\partial f}{\partial l} \Big|_{x=x^{(0)}, l=l^{(0)}}$$

$$\vec{r} = \text{residuals}$$

$$\vec{w} = f(x^{(0)}, l^{(0)})$$

For the ellipse model, the design matrices are,

$$\mathbf{A} = \begin{bmatrix} \frac{\partial f}{\partial a} & \frac{\partial f}{\partial b} & \frac{\partial f}{\partial d_x} & \frac{\partial f}{\partial d_z} & \frac{\partial f}{\partial d\alpha} \end{bmatrix}$$

$$\frac{\partial f}{\partial a} = -\frac{2(x \cos \alpha + d_x)^2}{a^3}$$

$$\frac{\partial f}{\partial b} = -\frac{2(z \sin \alpha + d_z)^2}{b^3}$$

$$\frac{\partial f}{\partial d_x} = \frac{2(x \cos \alpha + d_x)}{a^2}$$

$$\frac{\partial f}{\partial d_z} = \frac{2(z \sin \alpha + d_z)}{b^2}$$

$$\frac{\partial f}{\partial \alpha} = -\frac{2(x \cos \alpha + d_x)x \sin \alpha}{a^2} + \frac{2(z \sin \alpha + d_z)z \cos \alpha}{b^2}$$

$$\mathbf{B} = \begin{bmatrix} \frac{\partial f}{\partial x} & \frac{\partial f}{\partial z} \end{bmatrix}$$

$$\frac{\partial f}{\partial x} = -\frac{2(x \cos \alpha + d_x)x \sin \alpha}{a^2}$$

$$\frac{\partial f}{\partial z} = \frac{2(z \sin \alpha + d_z)z \cos \alpha}{b^2}$$

with a new row in \mathbf{A} and \mathbf{B} for each new observation. The circle model design matrix \mathbf{A} is,

$$\mathbf{A} = \begin{bmatrix} \frac{\partial f}{\partial R} & \frac{\partial f}{\partial d_x} & \frac{\partial f}{\partial d_z} \end{bmatrix}$$

$$\frac{\partial f}{\partial R} = -2R$$

$$\frac{\partial f}{\partial d_x} = 2(x + d_x)$$

$$\frac{\partial f}{\partial d_z} = 2(z + d_z)$$

and \mathbf{B} is,

$$\mathbf{B} = \begin{bmatrix} \frac{\partial f}{\partial x} & \frac{\partial f}{\partial z} \end{bmatrix}$$

$$\frac{\partial f}{\partial x} = 2(x + d_x)$$

$$\frac{\partial f}{\partial z} = 2(z + d_z)$$

The solution $\vec{\delta}$, is obtained from the following formulation,

$$\vec{\delta} = -(\mathbf{A}^T \mathbf{M} \mathbf{A})^{-1} \cdot \mathbf{A}^T \mathbf{M} \vec{w} \quad (2-4)$$

$$\text{where; } \mathbf{M} = (\mathbf{B} \mathbf{C}_l \mathbf{B}^T)^{-1}$$

\mathbf{C}_l covariance matrix of the observations

The corresponding covariance matrix for the estimated unknowns is given by,

$$\mathbf{C}_\delta = (\mathbf{A}^T \mathbf{M} \mathbf{A})^{-1} \quad (2-5)$$

The estimated residuals for the pipe cross section are used for anomaly detection and are computed by,

$$\vec{r} = -\mathbf{C}_l \mathbf{B}^T \mathbf{M} (\mathbf{A} \vec{\delta} + \vec{w}) \quad (2-6)$$

2.3 Chainage and Velocity

Velocity information computed from odometer wheels bounds the errors which occur in the time integration of the inertial data. At the same time these sensors provide a system chainage for the pig through its travel down the pipeline. The hinged wheels maintain contact with the pipe wall by spring tension as shown in Figure 2-8. The pivot shown in the figure allows the wheels an additional degree of freedom to maintain a tangential orientation when the pig is negotiating bends.

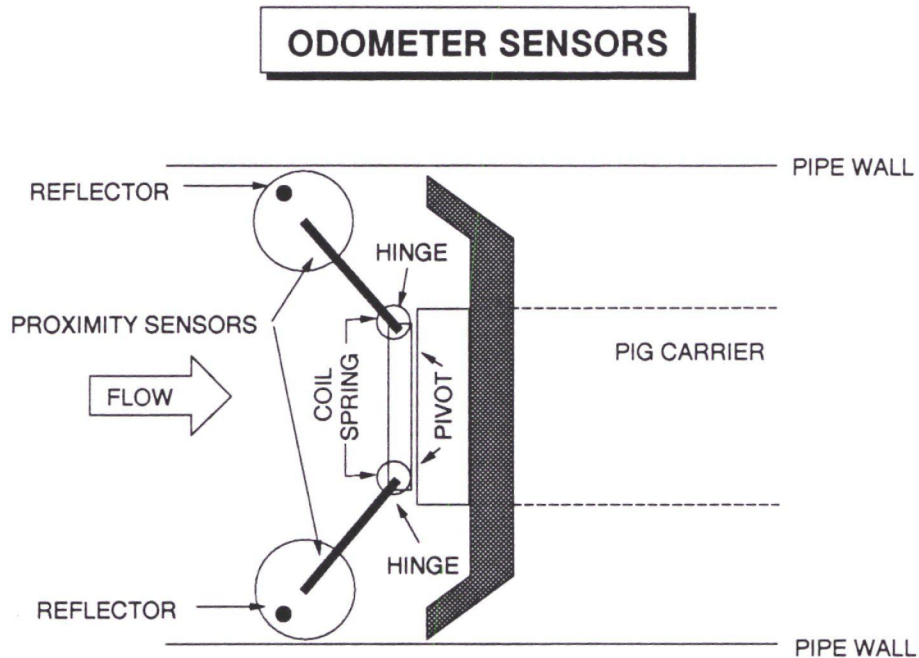


Figure 2-8. Odometer Sensors

Continuous checking between the two odometer wheels (or four, depending on configuration) determines odometer wheel slippage and is corrected. The redundancy also allows for relative scale estimation between the wheels. The velocity processing for the odometer wheels makes use of the redundancy to compute the best velocity possible for use as input observations for the Kalman filter. The along track velocity v_a is computed by using the recorded times of the reflectors passing by the proximity sensor as shown in Figure 2-8. The measured circumference of the wheel Δl over time interval Δt yields the velocity for each wheel. Opposing wheels are averaged to compute the centreline chainage and velocity of the pig.

2.4 Weld Detect

Circumferential weld detect sensors are mounted in one of the pig rubbers which sense the change in material properties of the pipe wall caused by the weld. The output of these sensors correlates the pig data to as-built plans while building a log of pipe joints for future comparisons. In epoch-to-epoch measurements, the historical information on weld separation provides an indication on the structural integrity of the pipeline by providing an estimate of the axial forces acting on the pipeline. A measurement accuracy of $\pm 1\text{cm}$ over a 20m

length of pipe would detect axial strains to +/- 500 $\mu\epsilon$. This is useful information for further structural reliability analysis and helps predict problem areas (Pare et al, 1989).

3 MATHEMATICAL MODELS

The aim of the pipeline deformation survey is the detection of critical curvatures and changes of length in the pipeline (the local problem), and the geodetic positioning of any location where these quantities exceed some design specification indicative of potential failure the (global problem).

The strapdown inertial measurement unit provides accurate profiling trajectory information in the local sense for several reasons. Firstly, it will directly experience, in the raw gyro and accelerometer outputs any rotations due to curvature of the pipeline. Secondly, output is at a high rate, in this case 16 Hz, hence profiles can be produced with a dense number of points. For the curvatures under consideration, these being in the order of 100m bend radius (and smaller) over 2m, a low accuracy strapdown INS (gyro drift $10^\circ/\text{hr}$) is sufficient in delivering this curvature requirement. This amounts to $10''/\text{s}$ which is well below the quantization level of the H778 gyros.

There are basically two ways to determine the curvature of a pipeline using strapdown systems, (1) by cross track acceleration (centrifugal force), or (2) by cross track angular velocity. Low accuracy systems are not accurate enough to use their acceleration output to determine the long radius of curvature required. Therefore, the angular velocity information is used. However, the acceleration is necessary to orientate the curve with respect to the vertical (Knickmeyer, 1988).

The objective then can be summarized as; computation of local trajectory information in terms of horizontal and vertical curvature and the determination of position and orientation of the pipeline pig.

3.1 Overview of Modelling Tasks

The modelling tasks for processing the specific force and angular rates measured by the strapdown INS are illustrated in Figure 3-1. The mechanization of the system output is formulated in a local-level navigation frame. The first step is executed by the calibration-/alignment module of this system, which determines the initial orientation and state of the system. From there, navigation in the local-level frame is performed. The body sensed specific forces are rotated to the local-level frame by means of the gyro updated transformation matrix. Removing the sensed gravity and Coriolis accelerations and integration of this acceleration supplies the velocity and position of the system. The Kalman filter is used

to control the inherent errors of the strapdown sensors, such as gyro drifts, accelerometer biases and misalignments by using the external observation information from velocity sensors. These main processing modules are described in the sections to follow, each one referenced by stream or number (1-14).

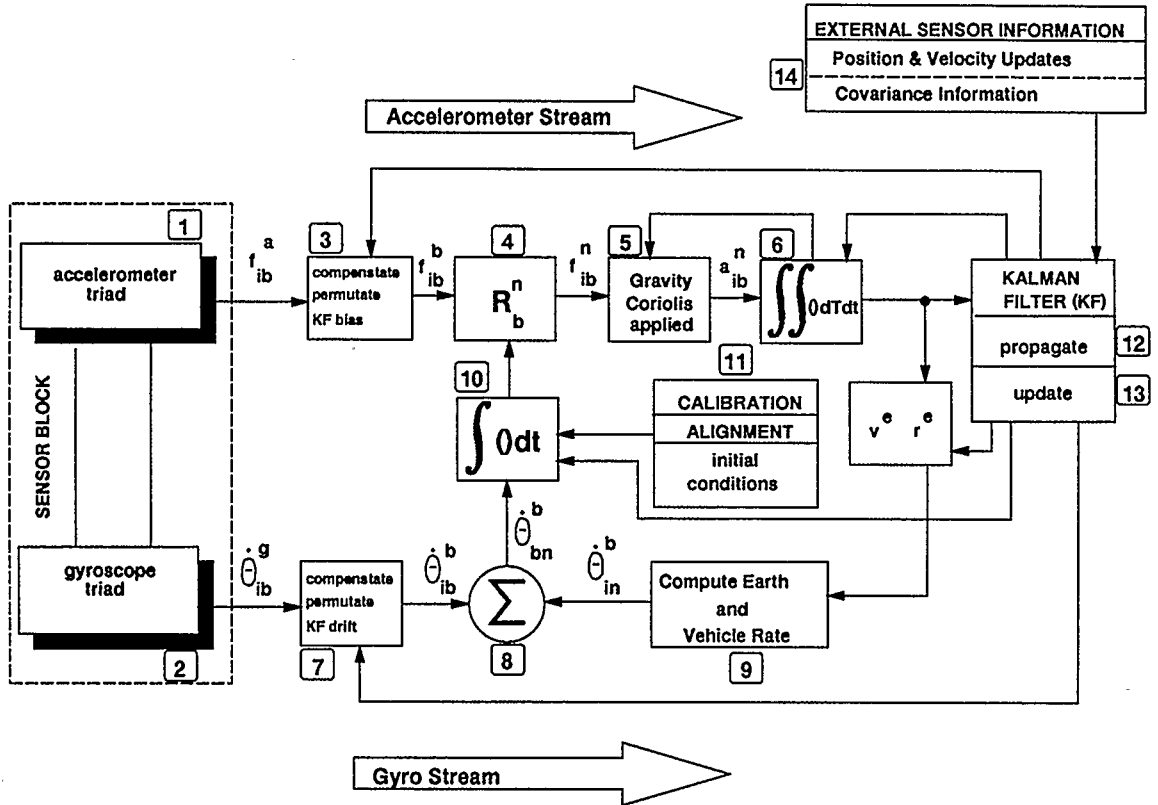


Figure 3-1. Local-level Strapdown Mechanization

Before modelling descriptions are given, it is important to define the coordinate reference frames used in the models throughout this chapter. They define the relationships between measurement and navigation quantities.

3.2 Reference Frames

Inertial navigation involves many reference frames and transformations between these frames in order to produce navigation quantities. A total of five frames are introduced, each one orthogonal, and right handed. For consistency throughout the document, each frame is designated by a single lower case letter.

Inertial Frame (i frame: x^i, y^i, z^i)

All sensor measurements of the strapdown INS are made with respect to inertial space, defined as a non-rotating and non-accelerating frame. Effects such as the earth's revolution around the sun and gravitational forces of the sun and moon fortunately are below the measurement sensitivity of most practical navigation systems (Britting, 1971).

The origin of an operational inertial frame is defined as the mass centre of the earth, with the primary axis aligned with the vernal equinox and the tertiary axis aligned with the spin axis of the earth as shown in the adjacent Figure 3-2a.

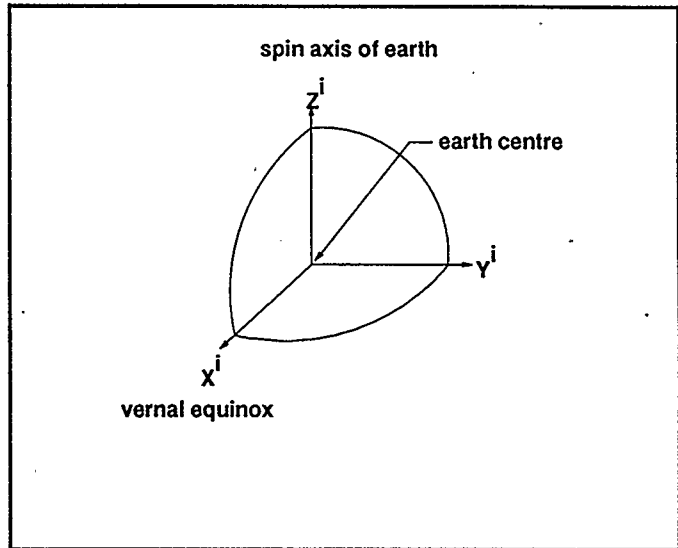


Figure 3-2a. Inertial Reference Frame

Earth Frame (e frame: x^e, y^e, z^e)

The earth frame, as the inertial frame, has its origin at the mass centre of the earth. It is fixed to the earth and at time $t=0$, the start of navigation, it is assumed coincident with the inertial frame. The primary axis is aligned with the local meridian and tertiary axis coincident with the spin axis of the earth.

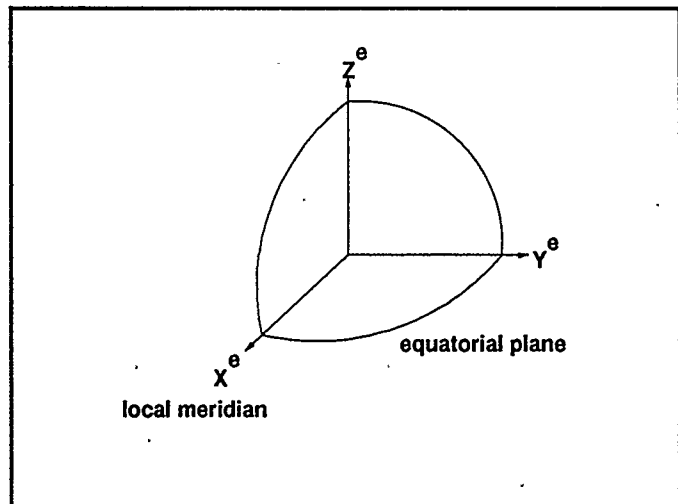


Figure 3-2b. Earth Frame

Local-level Frame (n frame: x^n, y^n, z^n)

The local-level frame origin is at the system location. The secondary axis points north and the tertiary axis is normal to the reference ellipsoid pointing outwards.

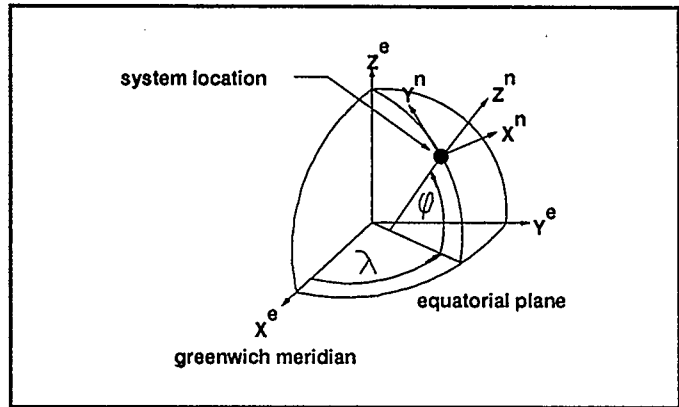


Figure 3-2c. Local-level Frame

Sensor Block Frame (p frame: x^p, y^p, z^p)

The origin of the sensor block frame is effectively the intersection of the sensitive axes of the accelerometer triad. The primary axis of the H778 is the longitudinal axis of the body and the secondary axis is lateral. In the event that the axes do not intersect, size effect compensation may be implemented to handle this.

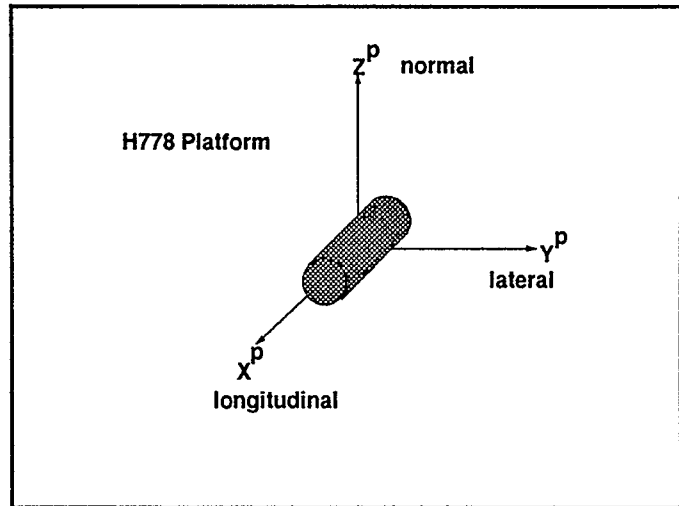


Figure 3-2d. Sensor Block Frame

Body Frame (b frame: x^b, y^b, z^b)

This frame is the observation frame used in the processing system. All computations are based on this frame with the primary axis lateral and the secondary axis longitudinal. This provides the familiar pitch (lateral), roll (longitudinal), and yaw (normal) components of vehicle movements.

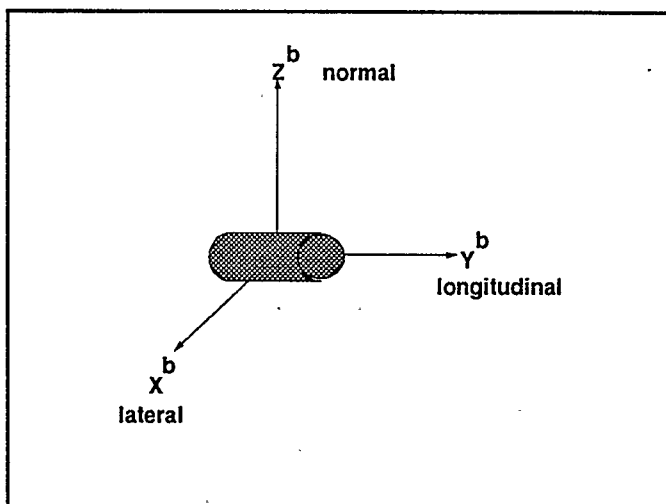


Figure 3-2e. Body Frame

The difference between the sensor block frame and the body frame is axis definition. The axis transformation allows for standardization of any strapdown INS to the body frame or computational frame in which all measurements are defined. Different strapdown models or different manufacturers may define the sensor axes of the gyros and accelerometers in various orientations. For example, the H778 requires a simple 90° positive rotation about the z^p axis to transform the outputs $\Delta\vec{\Theta}^p$ and $\vec{f}^p \Delta t$ to the body frame. The transformation operation is,

$$\vec{f}^b \Delta t = \mathbf{R}_p^b \vec{f}^p \Delta t \quad (3-1a)$$

$$\Delta\vec{\Theta}^b = \mathbf{R}_p^b \Delta\vec{\Theta}^p \quad (3-1b)$$

where;

$$\mathbf{R}_p^b = \begin{bmatrix} 0 & -1 & 0 \\ 1 & 0 & 0 \\ 0 & 0 & 1 \end{bmatrix}$$

Refer to Figure 3-2d and Figure 3-2e for an illustration.

3.3 Calibration / Alignment

The process of calibration is the determination of an initial set of strapdown sensor bias and drift errors. This set of errors provides an initial estimate for correcting the output of the

system. Alignment is the process of determining the angular relationship of the body and the local-level frame. This relationship is necessary in order to start the navigation and provide navigation output in the earth frame. Refer to Figure 3-1, function (11).

The approach used to calibrate and align the system is a modification of the analytical technique described by (Britting, 1971). This approach can only be used in the most benign applications, since any movement, vibration, swaying, etc., during the static alignment period would corrupt the measurements and observation of earth rate and gravity would be inaccurate. The effect of these disturbances would be a function of their magnitude and frequency. In the application of pipeline pigging, generally the alignment site is stable with the exception of vibration caused by large neighboring compressor or pump stations.

Adjustment Procedure

The basis of this process is to measure the components of gravity by the accelerometers, and to measure the components of earth rate by the gyros, and relate these observations by means of a transformation matrix, to the local-level gravity and earth rate components for the particular geographic location of the system. The static observation set(s) collected, span a certain time interval large enough for estimating biases and drifts. A typical time interval is 10 minutes. The observation sets are collected with the system in various orientations to aid in the estimation of the sensor errors.

The development of the models is based on the formulae given by (Britting, 1971) for the body sensed specific force \vec{g}^b and angular rates $\vec{\omega}_{ie}^b$,

$$\begin{aligned}\vec{g}^b &= \mathbf{R}_n^b \vec{g}^n \\ \vec{\omega}_{ie}^b &= \mathbf{R}_n^b \vec{\omega}_{ie}^n\end{aligned}$$

The functional relationship of the unknowns x , and observations l , is written by combining these formulae with the addition of bias and drifts terms,

$$f(x, l) = \mathbf{R}_n^b \begin{bmatrix} \vec{g}^n & \vec{\omega}_{ie}^n \end{bmatrix} - \begin{bmatrix} \vec{g}^b & \vec{\omega}_{ie}^b \end{bmatrix} - \begin{bmatrix} \vec{a}^b & \vec{b}^b \end{bmatrix} \quad (3-2)$$

The first term of Equation 3-2 transforms the computed earth model parameters of gravity \vec{g}^n , and earth rotation rate $\vec{\omega}_{ie}^n$, to the body frame via the local-level to body frame transformation matrix \mathbf{R}_n^b . The gravity vector \vec{g}^n is approximated by $\vec{\gamma}^n = [0, 0, \gamma]$. The second term contains the observations, where $\Delta \vec{v}$ are the velocity increments due to the

gravity vector and $\Delta\bar{\Theta}$ are angular increments due to the earth rate. The last term contains the estimate of accelerometer biases and gyro drifts of the system. The observation equation in expanded form is

$$f(x, l) = \mathbf{R}_n^b \begin{bmatrix} 0 & 0 \\ 0 & \omega_e \cos \phi \\ \gamma & \omega_e \sin \phi \end{bmatrix} - \begin{bmatrix} \Delta v_x^b & \Delta \Theta_x^b \\ \Delta v_y^b & \Delta \Theta_y^b \\ \Delta v_z^b & \Delta \Theta_z^b \end{bmatrix} - \begin{bmatrix} b_x^b & d_x^b \\ b_y^b & d_y^b \\ b_z^b & d_z^b \end{bmatrix} \quad (3-3)$$

The unknowns in the adjustment are; the accelerometer biases b , gyro drifts d , and the attitude angles of pitch (Θ), roll (ϕ), and yaw (ψ) contained in the transformation matrix \mathbf{R}_n^b defined in §3.4.3. The observations are $\Delta\bar{v}$ and $\Delta\bar{\Theta}$. Using this model, two modes of adjustment exist; alignment only, and combined calibration/alignment. In the case where only one static observation set is possible, the following dimensionality of the adjustment exists; unknowns (u) = 3 (one attitude set, no bias or drift estimation), observations (n) = 6 ($\Delta\bar{v}^b$, $\Delta\bar{\Theta}^b$), models (m) = 6. In order to estimate the biases and drifts, a minimum of two observation sets must be collected. The dimensionality would be; $n = 12$, $u = 12$, $m = 12$, since the solution is for two sets of system orientation angles. The vector of unknowns for the combined adjustment in the general case is,

$$\bar{\delta} = [b_x^b \ b_y^b \ b_z^b \ d_x^b \ d_y^b \ d_z^b \ \theta_1 \ \phi_1 \ \psi_1 \ \cdot \ \cdot \ \cdot \ \theta_k \ \phi_k \ \psi_k]^T \quad (3-4)$$

and the corresponding observation sets (1 to k) are the compensated accelerometer and gyro outputs (§3.4.1),

$$\bar{l} = \begin{bmatrix} \Delta\bar{v}_1^b \\ \Delta\bar{\Theta}_1^b \\ \cdot \\ \cdot \\ \cdot \\ \Delta\bar{v}_k^b \\ \Delta\bar{\Theta}_k^b \end{bmatrix} \quad (3-5)$$

where $\mathbf{R} = \mathbf{R}_b^n$, and one set of equations is obtained for each orientation.

The specific observation equations are written as,

$$f(x, l)_1 = R_{31} \cdot \gamma - [\Delta v_x^b + b_x^b] \quad (3-6)$$

$$f(x, l)_2 = R_{32} \cdot \gamma - [\Delta v_y^b + b_y^b] \quad (3-7)$$

$$f(x, l)_3 = R_{33} \cdot \gamma - [\Delta v_z^b + b_z^b] \quad (3-8)$$

$$f(x, l)_4 = R_{21} \cdot \omega_e \cos \phi + R_{31} \cdot \omega_e \sin \phi - [\Delta \Theta_x^b + d_x^b] \quad (3-9)$$

$$f(x, l)_5 = R_{22} \cdot \omega_e \cos \phi + R_{32} \cdot \omega_e \sin \phi - [\Delta \Theta_y^b + d_y^b] \quad (3-10)$$

$$f(x, l)_6 = R_{23} \cdot \omega_e \cos \phi + R_{33} \cdot \omega_e \sin \phi - [\Delta \Theta_z^b + d_z^b] \quad (3-11)$$

The least squares solution of this model is given by formula (2-3) to (2-6) with

$$\mathbf{A} = \frac{\partial f}{\partial x} \Big|_{x=x^{(0)}, l=l^{(0)}} \quad (3-12a)$$

where,

$$\mathbf{A} = \begin{bmatrix} -1 & 0 & 0 & 0 & 0 & 0 & \frac{\partial R_{31}}{\partial \Theta} \gamma & \frac{\partial R_{31}}{\partial \phi} \gamma & \frac{\partial R_{31}}{\partial \psi} \gamma \\ 0 & -1 & 0 & 0 & 0 & 0 & \frac{\partial R_{32}}{\partial \Theta} \gamma & \frac{\partial R_{32}}{\partial \phi} \gamma & \frac{\partial R_{32}}{\partial \psi} \gamma \\ 0 & 0 & -1 & 0 & 0 & 0 & \frac{\partial R_{33}}{\partial \Theta} \gamma & \frac{\partial R_{33}}{\partial \phi} \gamma & \frac{\partial R_{33}}{\partial \psi} \gamma \\ 0 & 0 & 0 & -1 & 0 & 0 & \frac{\partial R_{21}}{\partial \Theta} \omega_N + \frac{\partial R_{31}}{\partial \Theta} \omega_U & \frac{\partial R_{21}}{\partial \phi} \omega_N + \frac{\partial R_{31}}{\partial \phi} \omega_U & \frac{\partial R_{21}}{\partial \psi} \omega_N + \frac{\partial R_{31}}{\partial \psi} \omega_U \\ 0 & 0 & 0 & 0 & -1 & 0 & \frac{\partial R_{22}}{\partial \Theta} \omega_N + \frac{\partial R_{32}}{\partial \Theta} \omega_U & \frac{\partial R_{22}}{\partial \phi} \omega_N + \frac{\partial R_{32}}{\partial \phi} \omega_U & \frac{\partial R_{22}}{\partial \psi} \omega_N + \frac{\partial R_{32}}{\partial \psi} \omega_U \\ 0 & 0 & 0 & 0 & 0 & -1 & \frac{\partial R_{23}}{\partial \Theta} \omega_N + \frac{\partial R_{33}}{\partial \Theta} \omega_U & \frac{\partial R_{23}}{\partial \phi} \omega_N + \frac{\partial R_{33}}{\partial \phi} \omega_U & \frac{\partial R_{23}}{\partial \psi} \omega_N + \frac{\partial R_{33}}{\partial \psi} \omega_U \end{bmatrix}$$

using the components of earth rotation rate $\omega_N = \omega_e \cos \phi$, $\omega_U = \omega_e \sin \phi$, and normal gravity γ .

$$\mathbf{B} = \frac{\partial f}{\partial l} \Big|_{x=x^{(0)}, l=l^{(0)}} = \mathbf{I} \quad (3-12b)$$

Noting that the \mathbf{B} matrix of Equation 3-12b is identity, this adjustment is classified as parametric and the solution (Equation 2-6) simplifies to,

$$\vec{\delta} = -(\mathbf{A}^T \mathbf{C}_l^{-1} \mathbf{A})^{-1} \cdot \mathbf{A}^T \mathbf{C}_l \vec{w}. \quad (3-13)$$

The corresponding covariance matrix for the estimated unknowns is given by,

$$\mathbf{C}_\delta = (\mathbf{A}^T \mathbf{C}_l^{-1} \mathbf{A})^{-1}. \quad (3-14)$$

The procedure described can be used for the coarse alignment phase for determining the orientation of the body frame with respect to the local-level frame, and the body frame sensor errors. In order to improve these initial estimates, a fine alignment process is carried out, again using a longer span of static data collected at the beginning of the survey campaign. The fine alignment uses zero velocity updates and position resets as observations in the Kalman filter which is described in §3.5.

3.4 Navigation / Mechanization

The basis for all subsequent modelling of the strapdown inertial system is Newton's second law of motion,

$$\vec{a}^i = \vec{f}^i + \vec{g}^i \quad (3-15)$$

where \vec{a}^i , \vec{f}^i , \vec{g}^i , represent acceleration, specific force, and gravitation in an inertial frame.

For a rotating reference earth frame, the development of the mechanization equations begins with (Britting, 1971),

$$\vec{a}^i = \mathbf{R}_e^i (\vec{a}^e + 2\Omega_{ie}^e \vec{v}^e + \Omega_{ie}^e \Omega_{ie}^e \vec{r}^e) \quad (3-16)$$

where \mathbf{R}_e^i is the transformation from earth to inertial frame and, Ω_{ie}^e is the skew symmetric form of the components of earth rotation rate. The first term of the equation \vec{a}^e , describes the kinematic acceleration in the earth frame. The second term $2\Omega_{ie}^e \vec{v}^e$, is known as Coriolis acceleration, which occurs when moving on a rotating earth frame. The last term $\Omega_{ie}^e \Omega_{ie}^e \vec{r}^e$ is the centripetal acceleration sensed due to the rotation of the earth frame with respect to the inertial frame.

Equation (3-16) can be written in terms of the local-level navigation frame as,

$$\vec{a}^i = \mathbf{R}_n^i (\vec{a}^n + (2\Omega_{ie}^n + \Omega_{en}^n) \vec{v}^n + \Omega_{ie}^n \Omega_{ie}^n \vec{r}^n) \quad (3-17)$$

by introducing the rotation rate of the local-level frame with respect to the earth frame Ω_{en}^n , commonly called "vehicle rate". This fundamental equation provides the basis for strapdown processing. An interesting comparison of mechanizations using equations 3-16 and 3-17 is given in (Wei and Schwarz, 1990).

One function of the mechanization algorithms is to maintain a direct relationship between the body frame, where the measurements are made by means of the gyro input, and the local-level navigation frame. Applying earth and vehicle rates to the sensed gyro measurements provides the net orientation change of the body frame with respect to the navigation frame. These values are used in the equation for the rate of change of the body frame with respect to the local-level frame $\dot{\mathbf{R}}_b^n$ in the differential form,

$$\dot{\mathbf{R}}_b^n = \mathbf{R}_b^n \boldsymbol{\Omega}_{bn}^b \quad (3-18)$$

This matrix is integrated to provide the updated transformation matrix which rotates the specific force measured by the accelerometers $\vec{f}^b \Delta t$ into the navigation frame (east, north, and up), where the physical quantities of gravity and Coriolis accelerations are removed. This vehicle acceleration is computed by taking the equation for specific force given in (Britting, 1971),

$$\vec{f}^n = \vec{v}^n + (2\boldsymbol{\Omega}_{ie}^n + \boldsymbol{\Omega}_{en}^n) \vec{v}^n - \vec{g}^n \quad (3-19)$$

and re-writing it for extraction of the local-level accelerations,

$$\vec{v}^n = \vec{f}^n - (2\boldsymbol{\Omega}_{ie}^n + \boldsymbol{\Omega}_{en}^n) \vec{v}^n + \vec{g}^n \quad (3-20)$$

to obtain velocity and position change through integration.

The algorithm descriptions to follow make use of these two fundamental equations (3-18,20) above. The basic design and sequence of processing for strapdown sensor data is presented in the following sections and will make constant reference to the Figure 3-1.

3.4.1 Compensation

Compensation of the raw strapdown data is the first step of the processing. Referring to Figure 3-1, both the accelerometer (1) and gyro (2) output are compensated in functions (3) and (7) respectively. Each sensor block has a unique set of calibration coefficients which are provided by the manufacturer and are dependent on the type of gyro used (eg. mechanical, laser, fibre optic, etc.). These coefficients are typically; accelerometer biases and scale factors, gyro drifts, mass unbalance, and "g" sensitive (acceleration) scale factors and are applied through formulation provided by the manufacturer. The algorithms involve scaling and similarity transformations to compute the incremental velocity and angles measured in the sensor block frame.

Input $\vec{\Delta\theta}$
 $\vec{f}\Delta t$

For each individual component the formula is,

$$\Delta\theta^p = \Delta\theta - (d) - \Delta\theta(sf) - \Delta f^g \Delta t(mus) - \Delta f_s^g \Delta t(mui) - |\Delta\theta|(sfb)$$

where; d drift error

sf scale factor

$\Delta f^g \Delta t$ compensated accelerometer output in gyro frame

mus mass unbalance along the spin axis

$\Delta f_s^g \Delta t$ component of the compensated accelerometer output along the gyro spin axis in the gyro frame

mui mass unbalance along the input axis

sfb scale factor unbalance

For each individual component the formula is,

$$\Delta f^p \Delta t = f \Delta t - (b) - \Delta f \Delta t(sf) - |\Delta f| \Delta t(sfb)$$

where; b bias error

sf scale factor

sfb scale factor unbalance

Output $\vec{\Delta\theta}^p$
 $\vec{f}^p \Delta t$

Compensation and transformation to body frame are applied to the accelerometer and gyro triad output by using the sensor block to body transformation is described in §3.1. In describing the remaining mechanization functions, one method is to separate the accelerometer and gyro processing into two streams as shown in Figure 3-1. Each stream is of course dependant on the other, but can be described in this manner. Reference to Kalman filter feedback will be made in this section although the complete filter description is only given in §3.5.

3.4.2 Accelerometer Stream

Bias Correction

The accelerometer bias correction \vec{b} is available as a feedback correction from the Kalman filter and applied in function (3) in Figure 3-1. Accelerometer biases for all three sensors are part of the estimated error state, which become available when using the Kalman filter (described in §3.5).

$$\begin{array}{ll}
 \text{Input} & \vec{f}_{ib}^b \Delta t \\
 \text{Formula} & \vec{f}_{ib}^b \Delta t = \vec{f}_{ib}^b \Delta t - \vec{b} \Delta t \\
 \text{Output} & \vec{f}_{ib}^b \Delta t
 \end{array} \tag{3-21}$$

Transformation

The specific force increments are rotated from the body frame to the local-level frame as shown in Figure 3-1, function (4). In the application of pipeline pigging, where dynamics are very low, the following first order approximation is suitable (Stieler and Winter, 1982).

$$\begin{array}{ll}
 \text{Input} & \vec{f}_{ib}^b \Delta t, \mathbf{R}_b^n \\
 \text{Formula} & \vec{f}_{ib}^n \Delta t = \mathbf{R}_b^n \vec{f}_{ib}^b \Delta t \\
 \text{Output} & \vec{f}_{ib}^n \Delta t
 \end{array} \tag{3-22}$$

Gravity and Coriolis

Specific force in a local-level reference frame equation (3-19) can be rewritten (Britting, 1971) as;

$$\vec{f}^n = \vec{v}^n + \left(2\vec{\omega}_{ie}^n + \vec{\omega}_{en}^n \right) \times \vec{v}^n - \vec{g}^n \tag{3-23}$$

The Coriolis correction component, $2\vec{\omega}_{ie}^n + \vec{\omega}_{en}^n$, of the equation uses directly the earth rate, and vehicle rate (as defined in the gyro stream) from the previous computation cycle.

The actual gravity vector \vec{g}^n , is approximated by the normal gravity vector $\vec{\gamma}^n = [0, 0, \gamma]$. Normal gravity for a chosen earth model, in this case the WGS84 (DMA Technical Report, 1987) model is obtained from:

$$\gamma = \gamma^e \left[\frac{1 + k \sin^2 \phi}{\sqrt{1 - e^2 \sin^2 \phi}} \right] - \gamma^a \quad (3-24)$$

$$\begin{aligned} \text{where; } \gamma^e &= 9.780\ 326\ 7715 \text{ m/s}^2 \\ k &= 0.001\ 931\ 851\ 353 \\ \gamma^a &= 0.3086 \cdot 10^{-5} \text{ h (ellipsoidal height)} \end{aligned}$$

This formulation is rigorous but slow to compute in comparison to some approximate formulas. This is not a major concern in a post processing mode such as the pig application.

Assuming alignment with the ellipsoidal normal, $\vec{\gamma}^n = [0, 0, \gamma]$ and neglecting gravity anomalies which are smaller than the measurement accuracy of this system, Figure 3-1 function (5) removes these accelerations by,

Input $\vec{\omega}_{ie}^n, \vec{\omega}_{en}^n, \vec{v}^n, \vec{r}^e$ are used to compute the angular rate and gravity quantities.

$$\text{Formula } \Delta \vec{v}^n = \vec{f}^n \Delta t - (2\Omega_{ie}^n + \Omega_{en}^n) \vec{v}^n \Delta t + \vec{g}^n \Delta t \quad (3-25)$$

Output $\Delta \vec{v}^n$

Local-level Velocity

The local-level velocity vector \vec{v}^n is updated with the current cycle velocity increment $\Delta \vec{v}^n$ in Figure 3-1, function (6) by,

$$\vec{v}^n = \vec{v}_{(0)}^n + \Delta \vec{v}^n \quad (3-26)$$

Velocity Transformation

Local-level velocity is transformed to the earth frame in function (6) by using the prime vertical and meridian radius of curvature, R_N and R_M respectively, in the following transformation matrix,

$$\mathbf{D} = \begin{bmatrix} (R_N + h) \cos \phi & 0 & 0 \\ 0 & (R_M + h) & 0 \\ 0 & 0 & 1 \end{bmatrix}$$

where;

$$R_M = \frac{a(1-e^2)}{W^3}$$

$$R_N = \frac{a}{W}$$

$$W = \sqrt{1-e^2 \sin^2 \phi}$$

Input \vec{v}^n , earth model

Formula $\vec{v}^e = \mathbf{D}^{-1} \vec{v}^n$ (3-27)

Output $\vec{v}^e = \{\dot{\lambda}, \dot{\phi}, \dot{h}\}^T$

Position

The earth frame position \vec{r}^e is computed by simple integration of the current velocity over the processing cycle Δt using the earth frame velocity (function (6)).

Input $\vec{r}_{(0)}^e, \vec{v}^e$, earth model

Formula $\vec{r}^e = \vec{r}_{(0)}^e + \vec{v}^e \Delta t$ (3-28)

Output $\vec{r}^e = \{\lambda, \phi, h\}^T$

Velocity Correction

The velocity errors $\delta \vec{v}^e$ estimated by the Kalman filter (§3.5) are applied at this point (a subset of the complete Kalman state vector), providing the updated velocity.

Input $\delta \vec{v}^e = \{\delta \hat{\lambda}, \delta \hat{\phi}, \delta \hat{h}\}^T$

Formula $\vec{v}^e = \vec{v}^e + \delta \vec{v}^e$ (3-29)

Position Correction

From the Kalman filter, estimates for position errors $\delta \vec{r}^e$ are applied to the current computed position (again, a subset of the complete Kalman state vector §3.5). The output is the corrected position.

Input $\delta \vec{r}^e = \{\delta \hat{\lambda}, \delta \hat{\phi}, \delta \hat{h}\}^T$

Formula $\vec{r}^e = \vec{r}^e + \delta \vec{r}^e$ (3-30)

3.4.3 Gyro Stream

Drift Correction

The drift correction \vec{d} is another subset of the Kalman filter error state vector. This correction is applied at every cycle, as is done with the biases in the accelerometer stream. See Figure 3-1 function (7) in the gyro stream.

$$\begin{array}{ll}
 \text{Input} & \Delta \bar{\Theta}_{ib}^b \\
 \text{Formula} & \Delta \bar{\Theta}_{ib}^b = \Delta \bar{\Theta}_{ib}^b - \vec{d} \Delta t \\
 \text{Output} & \Delta \bar{\Theta}_{ib}^b
 \end{array} \tag{3-31}$$

Earth Rate

Earth rotation rate ω_e amounts to approximately 15"/s, and is removed from the sensed angular rates. From (Britting, 1971) the components of earth rate are a function of latitude (ϕ), and are computed by an earth-to-local-level transformation matrix (ie. with $\lambda = 0$) to form the earth rate vector in the local-level frame by function (9).

$$\begin{array}{ll}
 \text{Input} & \vec{r}^e, \text{ earth model} \\
 \text{Formula} & \vec{\omega}_{ie}^n = \mathbf{R}_e^n \vec{\omega}^e \\
 & \text{where;} \\
 & \mathbf{R}_e^n = \begin{bmatrix} 1 & 0 & 0 \\ 0 & \sin \phi & -\cos \phi \\ 0 & \cos \phi & \sin \phi \end{bmatrix} \\
 & \vec{\omega}^{eT} = \{0, 0, \omega_e\}
 \end{array} \tag{3-32}$$

Vehicle Rate

Vehicle rate is the angular velocity of the local-level frame with respect to the earth frame caused by the relative movement of the two frames computed in function (9).

$$\begin{array}{ll}
 \text{Input} & \vec{v}^e, \vec{r}^e \\
 \text{Formula} & \vec{\omega}_{en}^n = \{-\dot{\phi}, \dot{\lambda} \cos \phi, \dot{\lambda} \sin \phi\}^T
 \end{array} \tag{3-33}$$

Direction Cosine Integration

Strapdown assemblies and gimballed inertial platforms differ in one significant aspect - the method of obtaining meaningful accelerometer information. The primary function of the gyros is to provide a known coordinate reference frame for the accelerometers, and for the gimballed system this is achieved mechanically by using feedback platform control to maintain the accelerometer triad in a known spatial attitude. Strapdown mechanization maintains reference for the accelerometers by performing numerical transformation of the body sensed specific force to the reference frame. The numerical transformation is continuously updated by gyro measured information to maintain the body to reference frame relationship.

The transformation algorithm may use direction cosines or quaternions. Quaternions are a 4 parameter representation of the direction cosine matrix and are used in many applications. The selection of the approach was in the past dictated by the characteristics of the interfacing computer and mission requirements (eg. real-time navigation and guidance) which were memory requirements and throughput. The following three tasks have to be considered: (1) basic integration and updating algorithm, (2) normalization and orthogonalization algorithms, (3) algorithms for conversion to the direction cosine matrix form needed for acceleration transformation and Euler angle extraction. The comparison of the two approaches is summarized well by (Savage, 1982) and contained in Table 3-1.

Table 3-1. Direction Cosine vs. Quaternion Comparison

TASK	Direction Cosine (DC)	Quaternion (QU)
1	3x3 matrix contains 9 elements, all of which are updated .	Updating algorithm simpler than DC, only 4 QU elements are updated. This results in memory and throughput savings.
2	Requires Condition Least Squares Adjustment (CLSA) to maintain normality and orthogonality.	Generally simpler than the DC approach, resulting in memory savings, and some throughput savings. This task is typically run at a much lower rate than the processing rate, minimizing the benefit.
3	DC matrix is used directly for acceleration transformation. Euler angles are extracted by simple equations..	DC must be formed in order to transform accelerations. This causes severe memory and throughput penalties since this operation takes place at high rates. Euler angles are extracted from the formed DC matrix as in the DC approach.

The trade-offs of the two approaches are almost equal. The choice was not dictated by throughput and memory requirements since all processing is done post mission. The direction cosine approach was favored because the quantities were intuitively much easier to interpret, which is a very important consideration when implementation and testing of the algorithms takes place.

The direction cosine approach in the gyro stream processing, uses the "net" attitude change in the body frame to update the current attitude. This value is the input in the direction cosine integration to update the R_n^b transformation matrix. First, the "net" attitude change is computed by removing the earth and vehicle rates from the sensed angular increment. This task takes place in function (8) of the flowchart in Figure 3-1.

$$\text{Formula } \overline{\omega}_{in}^n = \overline{\omega}_{ie}^n + \overline{\omega}_{en}^n \quad (3-34)$$

$$\Delta \overline{\Theta}_{in}^b = R_n^b \overline{\omega}_{in}^n \Delta t \quad (3-35)$$

$$\Delta \overline{\Theta}_{bn}^b = \Delta \overline{\Theta}_{ib}^b - \Delta \overline{\Theta}_{in}^b \quad (3-36)$$

From (Savage, 1982), the direction cosine matrix is updated using the following algorithm (applied in function (10)) which is rigorous if $\Delta \Theta / \Delta t$ was constant over the past interval,

$$R_{b_t}^n = R_{b_{t-1}}^n (I + s \Omega + c \Omega^2) \quad (3-37)$$

$$\text{where; } s = \frac{\sin \Delta \Theta}{\Delta \Theta}$$

$$c = \frac{1 - \cos \Delta \Theta}{\Delta \Theta^2}$$

$$\Delta \Theta^2 = (\Delta \Theta_{bn}^b)_x^2 + (\Delta \Theta_{bn}^b)_y^2 + (\Delta \Theta_{bn}^b)_z^2$$

$$\Omega = \begin{bmatrix} 0 & -(\Delta \Theta_{bn}^b)_z & (\Delta \Theta_{bn}^b)_y \\ (\Delta \Theta_{bn}^b)_z & 0 & -(\Delta \Theta_{bn}^b)_x \\ -(\Delta \Theta_{bn}^b)_y & (\Delta \Theta_{bn}^b)_x & 0 \end{bmatrix}$$

The direction cosine matrix is formed by a sequence of pitch, roll, and yaw rotations. The right handed positive rotation matrices are;

$$R_1(\Theta) = \begin{bmatrix} 1 & 0 & 0 \\ 0 & \cos \Theta & \sin \Theta \\ 0 & -\sin \Theta & \cos \Theta \end{bmatrix}$$

$$\mathbf{R}_2(\phi) = \begin{bmatrix} \cos \phi & 0 & -\sin \phi \\ 0 & 1 & 0 \\ \sin \phi & 0 & \cos \phi \end{bmatrix}$$

$$\mathbf{R}_3(\psi) = \begin{bmatrix} \cos \psi & \sin \psi & 0 \\ -\sin \psi & \cos \psi & 0 \\ 0 & 0 & 1 \end{bmatrix}$$

$$\mathbf{R}_n^b = \mathbf{R}_2(\phi)\mathbf{R}_1(\Theta)\mathbf{R}_3(\psi) \quad (3-38)$$

where;

$$\begin{aligned} R_{11} &= \cos \psi \cos \phi - \sin \psi \sin \Theta \sin \phi \\ R_{12} &= -\sin \psi \cos \Theta \\ R_{13} &= \cos \psi \sin \phi + \sin \psi \sin \Theta \cos \phi \\ R_{21} &= \sin \psi \cos \phi + \cos \psi \sin \Theta \sin \phi \\ R_{22} &= \cos \psi \cos \Theta \\ R_{23} &= \sin \psi \sin \phi - \cos \psi \sin \Theta \cos \phi \\ R_{31} &= -\cos \Theta \sin \phi \\ R_{32} &= \sin \Theta \\ R_{33} &= \cos \Theta \cos \phi \end{aligned}$$

with; $\mathbf{R}_b^n = \mathbf{R}_n^{bT}$

For details see (Wells, 1971). Pitch Θ , roll ϕ , and yaw ψ , may be extracted from the \mathbf{R}_b^n by the following,

$$\Theta = \sin^{-1}[R_{32}] \quad (3-39)$$

$$\phi = \tan^{-1} \left[\frac{-R_{31}}{R_{33}} \right] \quad (3-40)$$

$$\psi = \tan^{-1} \left[\frac{-R_{12}}{R_{22}} \right] \quad (3-41)$$

Orthonormalization

In order to ensure accuracy of the attitude updating computation technique, an outer loop self-consistency check is employed on the direction cosine matrix. This takes place after function (10), but before function (4) shown in Figure 3-1. This is used in order to ensure that properties of the direction cosine matrix are maintained ie. rows of the matrix are orthogonal (orthogonality condition) to each other and equal to unity in magnitude (normality

condition). The consistency check is performed at a much lower frequency (eg. at 2 seconds, or every 32 cycles @ 16 Hz) by examining the misclosure of the condition models of orthogonality and normality. If the check fails, the Condition Least Squares Adjustment (CLSA) is performed on the direction cosine matrix \mathbf{R}_b^n .

Condition Least Squares Adjustment

The condition equations are derived from the relationship,

$$f(l) = \mathbf{R}^T \mathbf{R} - \mathbf{I} = 0 \quad (3-42)$$

where \mathbf{R}_b^n has been replaced with \mathbf{R} for simplicity.

Taking advantage of the symmetry structure, 6 condition equations ($m=6$) are written to enforce the orthonormality on the 9 elements ($n=9$) of the \mathbf{R}_b^n matrix. From (Krakiwsky and Vanicek, 1982), the least squares solution is formulated. Since $u=0$ (unknowns), the generalized equation (2-3) is greatly simplified, and written as,

$$\mathbf{B}\vec{r} + \vec{w} = 0 \quad (3-43)$$

with the least squares estimated residuals determined by,

$$\vec{r} = -\mathbf{C}_r \mathbf{B}^T (\mathbf{B} \mathbf{C}_r \mathbf{B}^T)^{-1} \vec{w} \quad (3-44)$$

and resultant adjusted observations, the 9 elements of the direction cosine matrix computed by,

$$\vec{l} = \vec{l} + \vec{r} \quad (3-45)$$

where; $\mathbf{B} = \frac{\partial f}{\partial l} \Big|_{l=l^{(0)}}$

$$\vec{w} = f(l^{(0)}) \quad \text{misclosure}$$

$$\vec{r}, \mathbf{C}_r \quad \text{residuals, and input covariance matrix}$$

$$\vec{l} \quad \text{observations, 9 elements of the } \mathbf{R}_b^n \text{ matrix}$$

Attitude Update

The Euler angle reset uses the Kalman estimates for attitude corrections. This reset may be performed by two methods. The first approach is used when the pitch and roll angles as well as the attitude errors are small. In that case

$$\mathbf{R}_b^n = (\mathbf{I} - \mathbf{E})\overline{\mathbf{R}}_b^n \quad (3-46)$$

where; $\overline{\mathbf{R}}_b^n$ (with errors)

$$\mathbf{E} = \begin{bmatrix} 0 & -\varepsilon_U & \varepsilon_N \\ \varepsilon_U & 0 & -\varepsilon_E \\ -\varepsilon_N & \varepsilon_E & 0 \end{bmatrix}$$

When pitch and roll angles are large, the misorientation angles are approximated in two steps. The first step transforms the local-level states to body frame

$$\vec{\varepsilon}^b = \mathbf{R}_n^b \vec{\varepsilon}^n \quad (3-47)$$

The second step involves re-computing the Euler angles by,

$$\varepsilon_\theta = \varepsilon_z^b \sin \phi + \varepsilon_x^b \cos \phi \quad (3-48)$$

$$\varepsilon_\phi = \varepsilon_y^b - \tan \Theta [\varepsilon_z^b \cos \phi - \varepsilon_x^b \sin \phi] \quad (3-49)$$

$$\varepsilon_\psi = \sec \Theta [\varepsilon_z^b \cos \phi - \varepsilon_x^b \sin \phi]. \quad (3-50)$$

These computed corrections are applied directly to the Euler angles, but this formulation is singular in the case of pitch at +/- 90°. The direction cosine matrix is then reconstructed from the corrected Euler angles using equation (3-38). Resets occur after function (10) but before the transformation in function (4) (refer to Figure 3-1).

3.5 Kalman Filter

3.5.1 Introduction

The sensor errors of the strapdown INS can be either systematic and random in nature. Large, or constant systematic errors are estimated by the coarse calibration/alignment procedure described in §3.1 and provide initial estimates for the sensor errors. Time dependant changes in these errors are re-estimated by means of a Kalman filter. The errors, known as state errors, are first identified and defined in order to design the filter models for controlling the strapdown INS. The error states are listed as follows,

$$\vec{x} = \{\varepsilon_E \quad \varepsilon_N \quad \varepsilon_U \quad \delta\lambda \quad \delta\phi \quad \delta h \quad \delta\dot{\lambda} \quad \delta\dot{\phi} \quad \delta\dot{h} \quad d_x \quad d_y \quad d_z \quad b_x \quad b_y \quad b_z\}^T \quad (3-51)$$

where; $\varepsilon_E, \varepsilon_N, \varepsilon_U$ misorientation of the sensor block,

$\delta\lambda, \delta\phi, \delta h$	position errors,
$\delta\dot{\lambda}, \delta\dot{\phi}, \delta\dot{h}$	velocity errors,
d_x, d_y, d_z	gyro drifts,
b_x, b_y, b_z	accelerometer biases

The error equation development presents the set of homogeneous linear differential equations satisfying the equation,

$$\dot{\vec{x}} = \mathbf{F}\vec{x} + \vec{w} \quad (3-52)$$

where; $\dot{\vec{x}}$	rate of change of the state errors
\mathbf{F}	dynamics matrix
\vec{x}	state errors
\vec{w}	system noise

The derivation of the dynamics matrix follows that in (Britting, 1971) or (Wong, 1988).

Attitude States

The raw angular rates used in updating the direction cosine matrix are computed by,

$$\vec{\omega}_{nb}^b = \vec{\omega}_{ib}^b - \bar{\mathbf{R}}_n^b \vec{\omega}_{in}^n \quad (3-53)$$

$$\text{where; } \bar{\mathbf{R}}_n^b = \mathbf{R}_n^b (\mathbf{I} - \mathbf{E})$$

$$\mathbf{E} = \begin{bmatrix} 0 & -\varepsilon_U & \varepsilon_N \\ \varepsilon_U & 0 & -\varepsilon_E \\ -\varepsilon_N & \varepsilon_E & 0 \end{bmatrix}$$

The misalignment errors are now written as,

$$\delta\vec{\omega}_{nb}^b = \mathbf{R}_n^b \mathbf{E} \vec{\omega}_{in}^n - \bar{\mathbf{R}}_n^b \delta\vec{\omega}_{in}^n + \vec{d} \quad (3-54)$$

$$\text{where; } \vec{d} \quad \text{gyro drift}$$

By transforming the above equation from the body frame to the local-level frame by \mathbf{R}_b^n , and noting that $\delta\vec{\omega}_{nb}^n = \delta\varepsilon$,

$$\delta \varepsilon = -\Omega_{in}^n \varepsilon - \delta \vec{\omega}_{in}^n + \mathbf{R}_b^n \vec{a} \quad (3-55)$$

$$\text{where; } -\Omega_{in}^n = \begin{bmatrix} 0 & \omega_e \sin \phi & -\omega_e \cos \phi \\ -\omega_e \sin \phi & 0 & -\dot{\phi} \\ \omega_e \cos \phi & \dot{\phi} & 0 \end{bmatrix}$$

$$-\delta \vec{\omega}_{in}^n = \begin{bmatrix} -\delta \dot{\phi} \\ -(\omega_e + \dot{\lambda}) \sin \phi \delta \phi + \cos \phi \delta \dot{\lambda} \\ (\omega_e + \dot{\lambda}) \cos \phi \delta \phi + \sin \phi \delta \dot{\lambda} \end{bmatrix}$$

The above equation forms rows 1, 2, and 3 of the dynamics matrix, where $\omega = \omega_e + \dot{\lambda}$.

$$\mathbf{F}_{1,2,3} = \begin{bmatrix} 0 & \omega \sin \phi & -\omega \cos \phi & 0 & 0 & 0 & 0 & 1 & 0 & R_{11} & R_{12} & R_{13} & 0 & 0 & 0 \\ -\omega \sin \phi & 0 & -\dot{\phi} & 0 & \omega \sin \phi & 0 & -\cos \phi & 0 & 0 & R_{21} & R_{22} & R_{23} & 0 & 0 & 0 \\ \omega \cos \phi & \dot{\phi} & 0 & 0 & -\omega \cos \phi & 0 & -\sin \phi & 0 & 0 & R_{31} & R_{32} & R_{33} & 0 & 0 & 0 \end{bmatrix}$$

Position States

The rate of change of the coordinate states are directly part of the error state, and rows 4, 5, and 6 are formed from,

$$\begin{bmatrix} \delta \dot{\lambda} \\ \delta \dot{\phi} \\ \delta \dot{h} \end{bmatrix} = \begin{bmatrix} \delta \dot{\lambda} \\ \delta \dot{\phi} \\ \delta \dot{h} \end{bmatrix} \quad (3-56)$$

$$\mathbf{F}_{4,5,6} = \begin{bmatrix} 0 & 0 & 0 & 0 & 0 & 0 & 1 & 0 & 0 & 0 & 0 & 0 & 0 & 0 & 0 \\ 0 & 0 & 0 & 0 & 0 & 0 & 0 & 1 & 0 & 0 & 0 & 0 & 0 & 0 & 0 \\ 0 & 0 & 0 & 0 & 0 & 0 & 0 & 0 & 1 & 0 & 0 & 0 & 0 & 0 & 0 \end{bmatrix}$$

Velocity States

The formulation for the rate of change of the velocity states, as (Wong, 1988) points out, is by far the most involved. The derivation begins with the specific force equation (3-19),

$$\vec{f}^n = \vec{v}^n + (2\vec{\omega}_{ie}^n + \vec{\omega}_{en}^n) \times \vec{v}^n - \vec{g}^n$$

which is written for raw acceleration as,

$$\vec{v}^n = \vec{f}^n - \left(2\vec{\omega}_{ie}^n + \vec{\omega}_{en}^n\right) \times \vec{v}^n + \vec{g}^n \quad (3-57)$$

and expanded to include the misorientation and bias errors,

$$\vec{v}^n = (\mathbf{I} + \mathbf{E})\mathbf{R}_b^n(\vec{f}^b + \vec{b}) - (\Omega_{en}^n + 2\Omega_{ie}^n)\vec{v}^n + \vec{g}^n \quad (3-58)$$

where; \vec{b} accelerometer bias

From (Britting, 1971), perturbation techniques are used to linearize the nonlinear system of differential equations. This results in linear differential equations involving only the error quantities. The error in acceleration is written as,

$$\begin{aligned} \delta\vec{v}^n &= \mathbf{E}\vec{f}^n && \text{first term} \\ &- (\Omega_{en}^n + 2\Omega_{ie}^n)\delta\vec{v}^n && \text{second term} \\ &- \left(\delta\vec{\omega}_{en}^n + 2\delta\vec{\omega}_{ie}^n\right) \times \vec{v}^n && \text{third term} \\ &+ \mathbf{R}_b^n \delta\vec{b} && \text{fourth term} \\ &- \frac{\partial\vec{g}^n}{\partial h} \delta h && \text{fifth term} \end{aligned} \quad (3-59)$$

The first term is rewritten as

$$\mathbf{E}\vec{f}^n = \begin{bmatrix} 0 & f_U & -f_N \\ -f_U & 0 & f_E \\ f_N & -f_E & 0 \end{bmatrix} \begin{bmatrix} \epsilon_E \\ \epsilon_N \\ \epsilon_U \end{bmatrix}$$

The second term is constructed by summation of the skew-symmetric forms of the earth and vehicle rates,

$$\begin{bmatrix} 0 & (2\omega_e + \dot{\lambda}) \sin \phi & -(2\omega_e + \dot{\lambda}) \cos \phi \\ -(2\omega_e + \dot{\lambda}) \sin \phi & 0 & -\dot{\phi} \\ (2\omega_e + \dot{\lambda}) \cos \phi & \dot{\phi} & 0 \end{bmatrix} \begin{bmatrix} \delta v_E \\ \delta v_N \\ \delta v_U \end{bmatrix}$$

$$\begin{aligned} \text{substituting;} \quad v_E &= \dot{\lambda} R_N \cos \phi \\ v_N &= \dot{\phi} R_M \\ v_U &= \dot{h} \\ \omega &= \omega_e + \dot{\lambda} \end{aligned}$$

and assuming that $\omega_e \gg \dot{\lambda}$,

$$2\omega = (2\omega_e + \dot{\lambda})$$

the second term results in,

$$\begin{bmatrix} 0 & 2R_M\omega \sin \phi & -2\omega \cos \phi \\ -2R_N\omega \sin \phi \cos \phi & 0 & -\dot{\phi} \\ 2R_N\omega \cos^2 \phi & R_M\dot{\phi} & 0 \end{bmatrix} \begin{bmatrix} \delta\dot{\lambda} \\ \delta\dot{\phi} \\ \delta\dot{h} \end{bmatrix}$$

The third term summation and cross product results in,

$$\begin{bmatrix} 2v_U\omega \sin \phi + 2v_N\omega \cos \phi & -v_U \cos \phi + v_N \sin \phi & 0 \\ -2v_E\omega \cos \phi & -v_E \sin \phi & -v_U \\ -2v_E\omega \sin \phi & v_E \cos \phi & v_N \end{bmatrix} \begin{bmatrix} \delta\phi \\ \delta\dot{\lambda} \\ \delta\dot{\phi} \end{bmatrix}$$

Using the same substitutions define above, and the fact that products of velocities are relatively small, and the further simplifying fact that $\omega_e \gg (\dot{\phi}, \dot{\lambda}) \gg \dot{h}/R$, we arrive at,

$$\begin{bmatrix} 0 & 0 & 0 \\ -R_N\dot{\lambda} \cos \phi \sin \phi & 0 & 0 \\ R_N\dot{\lambda} \cos^2 \phi & \dot{\phi}R_M & 0 \end{bmatrix} \begin{bmatrix} \delta\dot{\lambda} \\ \delta\dot{\phi} \\ \delta\dot{h} \end{bmatrix}$$

Summation of the second and third terms results in,

$$\begin{bmatrix} 0 & 2R_M\omega \sin \phi & -2\omega \cos \phi \\ -R_N\omega \sin 2\phi & 0 & -\dot{\phi} \\ 2R_N\omega \cos^2 \phi & 2R_M\dot{\phi} & 0 \end{bmatrix} \begin{bmatrix} \delta\dot{\lambda} \\ \delta\dot{\phi} \\ \delta\dot{h} \end{bmatrix}$$

Converting acceleration errors to angular units by,

$$\begin{bmatrix} \delta\ddot{\lambda} \\ \delta\ddot{\phi} \\ \delta\ddot{h} \end{bmatrix} = \begin{bmatrix} \delta\dot{v}_E/R_N \cos \phi \\ \delta\dot{v}_N/R_M \\ \delta\dot{v}_U \end{bmatrix}$$

results in,

$$\begin{bmatrix} 0 & 2\omega \tan \phi & -\frac{2\omega}{R_N} \\ -\omega \sin 2\phi & 0 & -\frac{\dot{\phi}}{R_M} \\ 2R_N\omega \cos^2 \phi & 2R_M\dot{\phi} & 0 \end{bmatrix} \begin{bmatrix} \delta\dot{\lambda} \\ \delta\dot{\phi} \\ \delta\dot{h} \end{bmatrix}$$

The solution to this system of differential equations, assuming that the expectation of the system noise is zero, is written as,

$$\vec{x}_t = \Phi_{t,t-1} \vec{x}_{t-1} \quad (3-62)$$

where; \vec{x}_t state vector at time t

$\Phi_{t,t-1}$ transition matrix for time interval (t-1) to t

\vec{x}_{t-1} state vector at time (t-1)

This formulation provides the mechanism for error propagation of the state vector. The transition matrix is computed from the dynamics matrix by the matrix exponential,

$$\Phi = e^{F\Delta t} \quad (3-63)$$

which expanded into a Taylor series is,

$$\Phi_{t,t-1} = I + F\Delta t + 0.5FF\Delta t^2 + \dots \quad (3-64)$$

Considering the specific dynamics of this application, almost constant velocity and short time interval Δt used, the elements of the dynamics matrix experience relatively small changes, and can be assumed to be constant over the time interval. Thus the series is truncated to,

$$\Phi_{t,t-1} = I + F\Delta t \quad (3-65)$$

The propagated covariance matrix of the state vector is obtained by applying the covariance law, and considering system noise,

$$C_{x_t} = \Phi_{t,t-1} C_{x_{t-1}} \Phi_{t,t-1}^T + C_w \quad (3-66)$$

where; C_w covariance matrix derived from the spectral variance density matrix of the system noise

3.5.2 Velocity Updates

Updating the state vector can be accomplished in a number of different ways in this application. External sources of aiding are velocity (along track) by odometer wheels on an almost continuous basis. Coordinate control can be obtained from as-built plans and used by detecting the passage of the pig train through valves and other above ground identifiable

features. Typically these control point updates occur at roughly 10km intervals. In addition, distance updates can be obtained at frequent intervals by monitoring the consecutive passage of subsequent sets of pipe joints. The update equations for external observations are,

$$\vec{y} = \mathbf{H}\vec{x} + \vec{e} \quad (3-67)$$

where; \vec{y} the observations
 \mathbf{H} the Jacobian relating the observations to the states
 \vec{x} state vector
 \vec{e} measurement noise

The propagated state vector and its covariance matrix are estimated by the Kalman update equations,

$$\mathbf{K} = \mathbf{C}_x^{-1} \mathbf{H}^T (\mathbf{H} \mathbf{C}_x^{-1} \mathbf{H}^T + \mathbf{C}_y)^{-1} \quad (3-68)$$

$$\vec{x}^+ = \vec{x}^- - \mathbf{K}(\mathbf{H}\vec{x}^- - \vec{y}) \quad (3-69)$$

$$\mathbf{C}_x^+ = (\mathbf{I} - \mathbf{K}\mathbf{H})\mathbf{C}_x^- \quad (3-70)$$

where; \mathbf{K} gain matrix
 \mathbf{C}_y covariance matrix of the observations

The velocity observations obtained by odometers are typically at 1 Hz. To formulate the observation equations the following definitions are used,

$v^b = \{0 \ v_a \ 0\}^T$ where v_a denotes the measured along track velocity from the odometers.

$\tilde{v}^n = \{\tilde{v}_E \ \tilde{v}_N \ \tilde{v}_U\}^T$ quasi-observables in local-level frame

$\tilde{\tilde{v}}^n = \{\tilde{\tilde{v}}_E \ \tilde{\tilde{v}}_N \ \tilde{\tilde{v}}_U\}^T$ quasi-observables with misorientation errors

$\bar{v}^n = \{\bar{v}_E \ \bar{v}_N \ \bar{v}_U\}^T$ mechanization velocity in local-level frame

$\delta v = \{R_E \delta \lambda \ R_M \delta \phi \ \delta h\}^T$ velocity errors

$\epsilon = \{\epsilon_E \ \epsilon_N \ \epsilon_U\}^T$ misorientation errors

The basic observation equation is written by formulating the relationship of \tilde{v}^n with respect to the mechanization velocity and velocity errors,

$$\tilde{v}^n = \bar{v}^n - \delta v \quad (3-71)$$

Misorientation errors are included by,

$$\tilde{v}^n = \bar{\mathbf{R}}_b^n v^b = (\mathbf{I} + \mathbf{E}) \mathbf{R}_b^n v^b \quad (3-72)$$

which transforms to,

$$\tilde{v}^n = v^n + \mathbf{E} v^n \quad (3-73)$$

This can be rearranged to,

$$\tilde{v}^n = v^n + \tilde{\mathbf{V}} \mathbf{E} \quad (3-74)$$

$$\text{where; } \tilde{\mathbf{V}} = \begin{bmatrix} 0 & \tilde{v}_U & -\tilde{v}_N \\ -\tilde{v}_U & 0 & \tilde{v}_E \\ \tilde{v}_N & -\tilde{v}_E & 0 \end{bmatrix}$$

Substituting this equation into (3-70) gives,

$$\tilde{v}^n - \bar{v}^n = \tilde{\mathbf{V}} \mathbf{E} - \delta v \quad (3-75)$$

which is in the form of the general observation equation given in (3-67),

$$\vec{y} = \mathbf{H} \vec{x} + \vec{e}$$

where; \vec{x} state vector

\vec{e} observation noise

$$\text{and, } \vec{y} = \begin{bmatrix} \tilde{v}_E^n - \bar{v}_E^n \\ \tilde{v}_N^n - \bar{v}_N^n \\ \tilde{v}_U^n - \bar{v}_U^n \end{bmatrix}$$

$$\mathbf{H} = \begin{bmatrix} 0 & -\tilde{v}_U & \tilde{v}_N & 0 & 0 & 0 & 0 & R_M & 0 & 0 & 0 & 0 & 0 & 0 & 0 \\ \tilde{v}_U & 0 & -\tilde{v}_E & 0 & 0 & 0 & R_E & 0 & 0 & 0 & 0 & 0 & 0 & 0 & 0 \\ -\tilde{v}_N & \tilde{v}_E & 0 & 0 & 0 & 0 & 0 & 0 & 1 & 0 & 0 & 0 & 0 & 0 & 0 \end{bmatrix}$$

The covariance matrix \mathbf{C}_y , is formed by applying the covariance law to the original along track odometer velocity,

$$C_y = \overline{R}_b^n \begin{bmatrix} 0 & 0 & 0 \\ 0 & \sigma_a^2 & 0 \\ 0 & 0 & 0 \end{bmatrix} \overline{R}_n^b \quad (3-76)$$

In the context of the global problem, velocity update information is utilized to reduce velocity and position error growth. This is however, not enough to achieve the required position accuracy of 10m. Combining the positioning results from the system with the chainage provided by odometers and the position information obtained from detection of surface features such as valves, bends, etc., will usually result in a relative positioning of the pig to about 10m level. This accuracy is with respect to the nearest detectable feature. At the same time local trajectory information is sufficiently recovered from the mechanized angular rates. Locating critical curvatures with the above accuracy is considered more than adequate for the inspection and maintenance of operating pipelines.

3.6 Curvature

Curvature is used to assess and monitor the effects of pipe deformations caused by slope instability, movement of river crossings, thaw settlement, and frost heave. It is compared with the original as built curvature to provide initial structural parameters based on the bending effect of the pipeline.

The analysis of local trajectory information can be tied directly to the mechanization equations through utilization of differences in Euler angles and/or angular rates since even the large gyro drift rates of a low accuracy strapdown INS ($10^\circ/\text{hr}$) are orders of magnitude less than the curvatures we are concerned with for single and multi-run surveys.

Using the raw gyro rates, from (Knickmeyer, 1988), curvature and torsion formulas can be expressed as a function of the across track angular rates divided by the velocity, while inclination and azimuth (pitch and yaw) are a direct result of the strapdown mechanization providing the vertical and horizontal components of curvature respectively.

Differences in these quantities between epochs can be construed as horizontal and/or vertical curvature changes of the pipe. It can also be expressed by the deflection angle $\Delta\alpha$, see Figure 3-3. If the deflection angle exceeds some criteria it can be flagged as an area of potentially critical curvature. An illustration of this is given in a more elegant way in (Knickmeyer, 1988) utilizing the concepts of differential geometry. Figure 3-3 illustrates the geometric parameters of curvature.

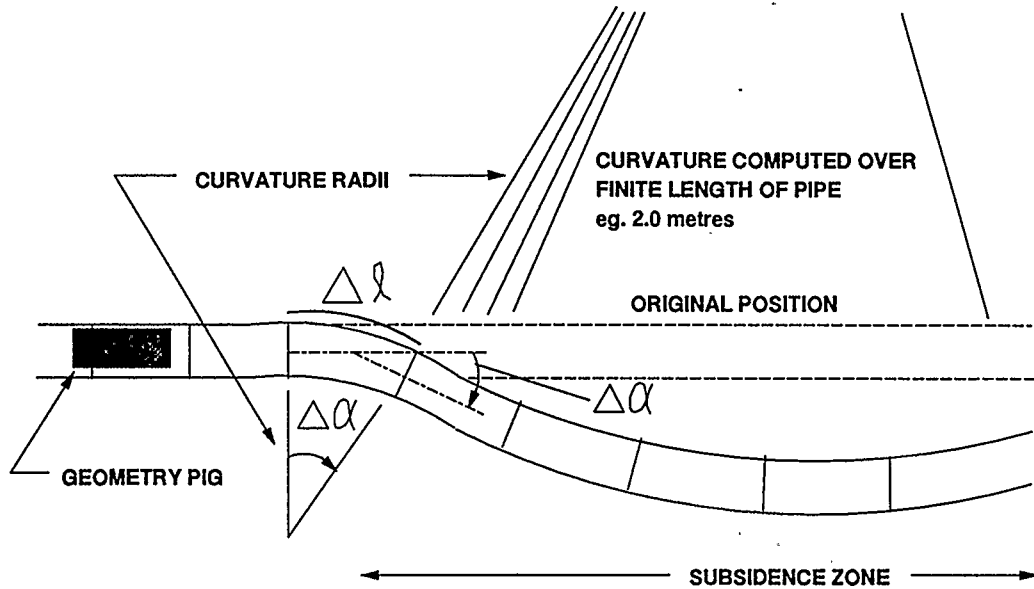


Figure 3-3. Pipeline Curvature

The method of expressing curvature κ directly as a function of the measured across track angular rates ω in the plane of the pipe cross section, and the velocity or distance travelled over a specified time interval Δt is formulated as,

$$\kappa = \Delta\alpha/\Delta l \quad (3-77)$$

$$\text{where; } \Delta\alpha = \sqrt{(\omega_x^b \Delta t)^2 + (\omega_z^b \Delta t)^2} / |v|$$

v = tangential velocity (from either the strapdown INS or odometer)

Δl = chord length

The definition of $\Delta\alpha$ implies that velocity over the time period Δt is constant. Curvature components may be examined at the raw data stage by using compensated angular and acceleration input. In order to resolve the angular body rates into horizontal and vertical curvature, an approximation for the body to local-level transformation matrix is computed. This is possible by using the output of the accelerometers to estimate the current pitch and roll orientation of the body frame by;

$$\vec{g}^n = \mathbf{R}_b^n \vec{g}^b \quad (3-78)$$

which is further expanded to (Knickmeyer, 1988),

$$\begin{bmatrix} 0 \\ 0 \\ -g \end{bmatrix}^n = \mathbf{R}_b^n \cdot \begin{bmatrix} g_x \\ g_y \\ g_z \end{bmatrix}^b = \mathbf{R}_b^n \cdot \begin{bmatrix} -f_x \\ -f_y + \ddot{x}_y \\ -f_z \end{bmatrix}^b \quad (3-79)$$

where; \ddot{x}_y = along track acceleration

The along track acceleration is minimized or zeroed by selecting a constant velocity section of data using the odometer information. This reduces most of the error in approximating pitch and roll angles.

Pitch angle of the system is given by;

$$\Theta = \sin^{-1}(g_x^b/g_z^b) \quad (3-80)$$

Roll angle of the system is given by;

$$\phi = \sin^{-1}(g_y^b/g) = \tan^{-1}(g_y^b/\sqrt{g_x^{b2} + g_z^{b2}}) \quad (3-81)$$

$$\text{where; } g = \sqrt{(g_x^b)^2 + (g_y^b)^2 + (g_z^b)^2}$$

Another approach in approximating the system orientation is to express directly \mathbf{R}_b^n by the measured specific force \vec{f}^b . An arbitrary local-level frame is defined (since yaw is not estimated) and the \mathbf{R}_b^n transformation matrix constructed as defined in §3.4.3,

$$\begin{aligned} R_{11} &= \cos \phi \\ R_{12} &= 0 \\ R_{13} &= \sin \phi \\ R_{21} &= \sin \Theta \sin \phi \\ R_{22} &= \cos \Theta \\ R_{23} &= -\sin \Theta \cos \phi \\ R_{31} &= -\cos \Theta \sin \phi \\ R_{32} &= \sin \Theta \\ R_{33} &= \cos \Theta \cos \phi \end{aligned}$$

The direction cosines of the local-level to body frame are expressed as a direct function of \vec{g} (3-78);

$$\vec{x}_n^b = \text{norm}(\vec{g}^b \times \vec{y}^b) \quad (3-82)$$

$$\vec{z}_n^b = \text{norm}(-\vec{g}^b) \quad (3-83)$$

The "y" component is computed by the cross-product of the "x" and "z" components,

$$\vec{y}_n^b = \text{norm}(\vec{z}_n^b \times \vec{x}_n^b) \quad (3-84)$$

$$\text{where; } \text{norm}(\vec{a}) = \vec{a} / |\vec{a}|$$

$$|\vec{a}| = \sqrt{a_x^2 + a_y^2 + a_z^2}$$

$$\vec{v} = \vec{a} \times \vec{b} = \begin{bmatrix} a_y b_z - a_z b_y \\ a_z b_x - a_x b_z \\ a_x b_y - a_y b_x \end{bmatrix}$$

$$\vec{y}^b = [0 \ 1 \ 0]^T$$

The columns of the \mathbf{R}_n^b are,

$$\vec{x}_n^b = \begin{bmatrix} -g_z^b / \Gamma \\ 0 \\ g_x^b / \Gamma \end{bmatrix} \quad (3-85)$$

$$\vec{z}_n^b = \begin{bmatrix} -g_x^b / g \\ -g_y^b / g \\ -g_z^b / g \end{bmatrix} \quad (3-86)$$

$$\vec{y}_n^b = \begin{bmatrix} -g_x^b g_y^b / (g\Gamma) \\ \Gamma / g \\ -g_y^b g_z^b / (g\Gamma) \end{bmatrix} \quad (3-87)$$

$$\text{where; } \Gamma = \sqrt{g_x^{b2} + g_z^{b2}}$$

Combining the columns from equations (3-85) through (3-87),

$$\mathbf{R}_n^b = [\vec{x}_n^b \ \vec{y}_n^b \ \vec{z}_n^b] \quad (3-88)$$

provides directly the transformation matrix. The raw gyro output may be used directly with this approximate transformation matrix to examine horizontal and vertical curvatures.

Precise curvature radii are computed from the mechanized Euler angles, pitch for vertical curvature, and yaw for horizontal curvature,

$$R_V = \frac{\Delta\theta}{\Delta l} \quad (3-89)$$

$$R_H = \frac{\Delta\psi}{\Delta l} \quad (3-90)$$

where; Δl = chord length

The computed radii from equations (3-89) and (3-90) are presented in terms of standardized curvature which includes the pipe radius in the formulation. Throughout this document curvature implies this standardized quantity. The computation is written as,

$$\kappa_V = R_{pipe}/R_V \times 100 \quad (3-91)$$

$$\kappa_H = R_{pipe}/R_H \times 100 \quad (3-92)$$

where a factor of 100 is used to express curvature in percent.

3.7 Computational Considerations

A suitable recording/processing rate must be chosen to meet hardware limitations, accuracy requirements, and fulfill the measurement spacing requirement of the moving pig in the pipeline. A simulation study was carried out in order to assess the errors associated with quantization levels, commutativity, and data recording rates. The simulation was designed on the basis of rotating a unit vector at various rates, constant and sinusoidal, with noise modulation, and comparing it to the orientation of a resultant analog vector orientation which was produced from rates at 1000Hz. This provides an estimate of the errors anticipated, and aids in a hardware design that can cope with the specified data rates.

The results for the data rate study are contained in Figure 3-4. Processing frequencies ranging from 512 Hz to 8 Hz were tested using the simulation technique discussed. At the very minimum 8 Hz was used, in order to provide the data point spacing with line speeds in the 0.5 to 2.0 m/s range. In order to minimize the potential errors, and keep them essentially below the quantization level of the system (25"), 16 Hz was selected as the data collection rate.

In order to anticipate the possible orientation errors arising from the quantization level of the H778 strapdown INS, the various recording/processing rates were examined. It can be

seen in Figure 3-5 that the errors in the complete recording range with the given dynamics of the pipeline environment were again at the level of quantization. No particular rate provided better results.

A commutativity study was conducted at the selected recording rate with no quantization and compared to the method proposed in (Savage, 1982). The results in Figure 3-6 show that the errors in commutativity of the three rotation matrices are identical and very closely approximate the approach of (Savage, 1982) for 16 Hz. The baseline for comparison was Savage at 100 Hz.

The conclusion of this simulation study was that the recording rate of 16 Hz with the given dynamics of the oil pipeline would not introduce errors greater than the quantization level of the system.

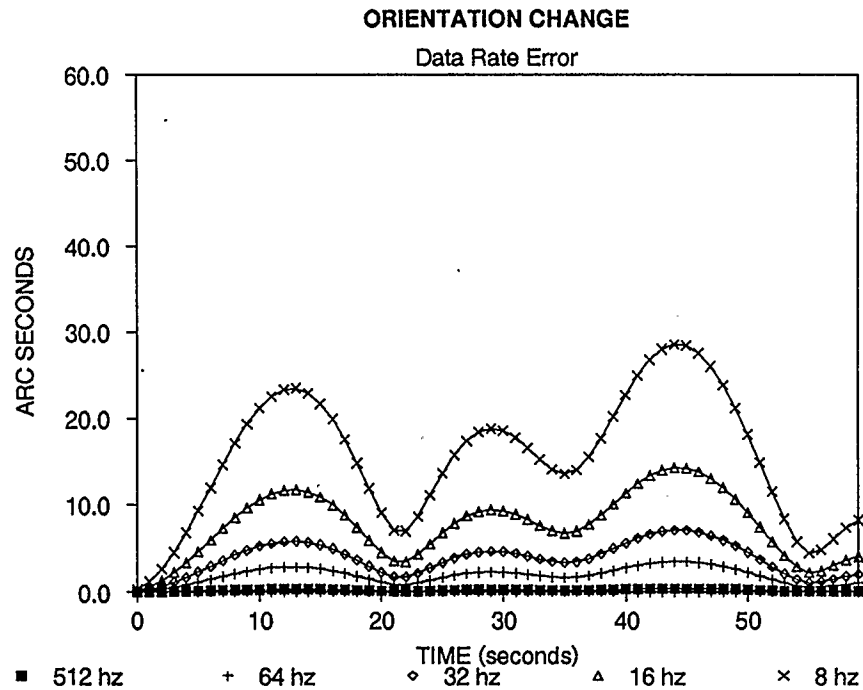


Figure 3-4. Effect of Data Rates on Attitude

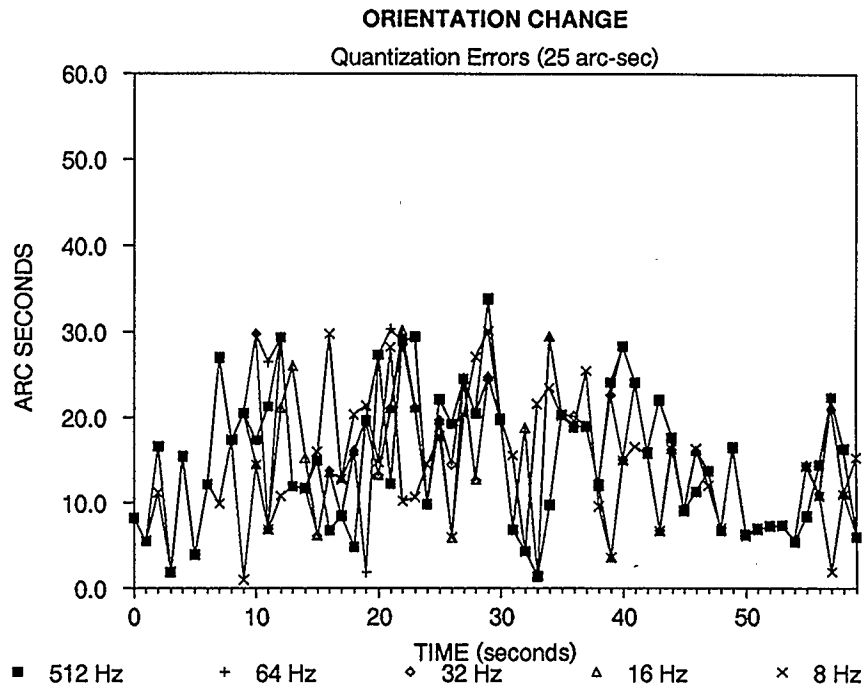


Figure 3-5. Effect of Quantization on Attitude

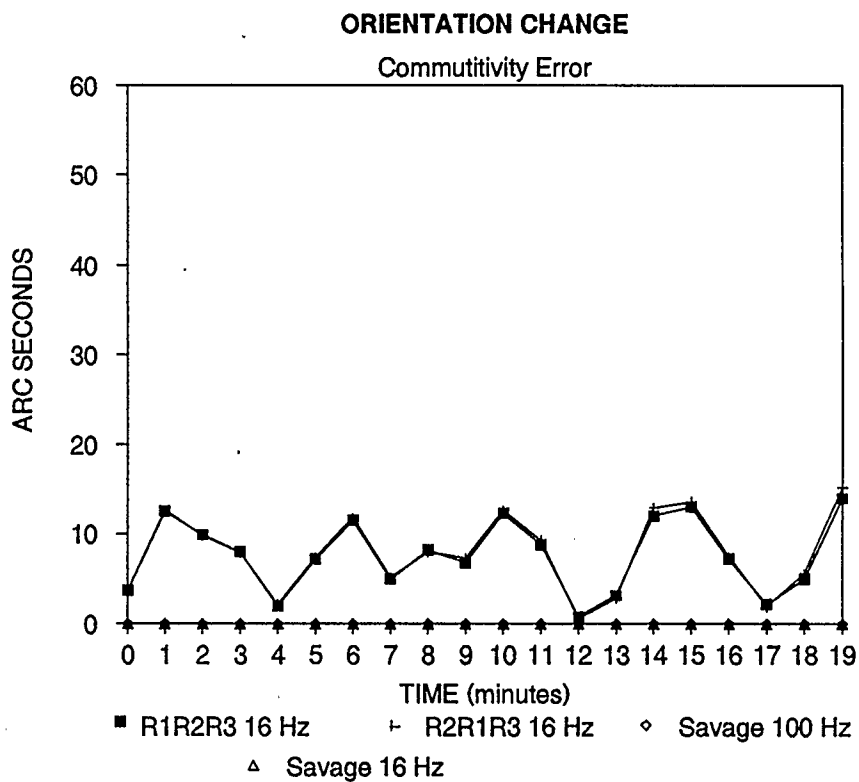


Figure 3-6. Effect of Commutativity on Attitude

4 PIPELINE MONITORING RESULTS

The geometry pig results are from Interprovincial Pipeline Company's (IPL) Norman Wells line which was constructed in 1984. The NPS-12 crude oil line is completely buried in sub-arctic terrain and extends from Norman Wells, NWT, to Zama, Alberta. Almost 80% of the line route is located in discontinuous permafrost where thaw settlement, frost heave, and permafrost slope stability are of concern (Nixon et al, 1984). In order to accurately monitor these phenomenon, IPL funded development of the geometry pig to measure curvature and location (Figure 1-1).

The results for the first 10km of this pipeline originating in Norman Wells, NWT are given. Analyses are presented for three separate runs of this section of the line. Comparisons of the three runs are made for assessing the accuracy and repeatability of the curvature and positioning capability.

With the overall success of the first geometry pigging tool, IPL funded further development of the geometry pig by adding caliper capabilities for measuring dents and ovality of an operating pipeline (Figure 1-2). This additional capability of the geometry pig is presented along with actual field verification of the caliper measurement accuracy from data collected on IPL's NPS-30 crude oil line in Eastern Canada.

4.1 Single Run Analysis

The initial, or single run, of a pipeline establishes the baseline from which the current "in-situ" geometry can be assessed. The position, curvature, and line features of dents and ovality, as well as valve locations, inside diameters (change in pipe wall thickness), and welds are logged. In addition to determining the baseline from which future surveys can be referenced, a detailed inventory and log of the line is produced. This provides the basis for subsequent deformation analysis and prediction of the pipeline response to the external forces causing the movement.

The results from the calibration, alignment, and Kalman filter performance of strapdown INS are described followed by navigation output and curvature results.

4.1.1 Alignment Analysis

The calibration and alignment procedure was described in §3.3 and involves collecting a number of static data sets in various orientations under the same system power-up. The orientations of these sets are typically one in each quadrant and are logged with the system

level. The system is then rolled 90°, then another 90° in the same direction. Pitching of the system is also done to whatever maximum inclination is possible, considering the system weighs approximately 300 Kg. The objective of this calibration is to estimate the gyro and accelerometer sensor errors by projecting the earth rotation rate and the local gravity vector on different orientations of the sensor triads, as well as computing the various orientations of the observation sets.

The resultant estimates for gyro drifts and accelerometer biases in the body frame from the calibration/alignment of runs 1, 2, and 3 are listed below. As can be seen in Tables 4-1 and 4-2, the biases and drifts are not constant from power-up to power-up and must be estimated for each run. The standard deviations are also large indicating the uncertainty of these values, which may be largely a function of the accelerometer inaccuracy and the quantization level of the sensors.

Table 4-1. Gyro Drift Estimation Results ("/s)

Run	Sets	d_x	σ	d_y	σ	d_z	σ
1	6	4.4	1.1	3.1	1.1	1.8	0.9
2	7	2.7	0.9	-2.2	1.5	0.5	1.0
3	7	5.6	0.7	0.3	0.7	-0.9	0.8

Table 4-2. Accelerometer Bias Estimation Results (m/s²/s)

Run	Sets	b_x	σ	b_y	σ	b_z	σ
1	6	0.0009	0.0007	-0.0322	0.0480	0.0004	0.0005
2	7	-0.0014	0.0006	-0.0013	0.0068	-0.0011	0.0009
3	7	-0.0032	0.0004	-0.0011	0.0300	0.0089	0.0005

As can be seen in the table above, the statistic for the y-axis accelerometer (b_y) is large with the exception of set 2. This clearly shows the effect of the inclined observation set collected in run 2.

To aid levelling, the system was rolled twice in all three cases. Run 2 was the only instance where one of the calibration sets was pitched up. As the table shows, large standard deviations on pitch as compared to roll exist in all runs except run 2. This is a function of the orientation

sets collected. In order to assess the levelling accuracy, navigation is carried out using the calibration/alignment solution for the static mission alignment data set with no velocity aiding. Given a perfect alignment, the resultant velocity and position errors would be zero. The velocity and position errors for runs 1, 2, and 3 are shown in Figures 4-1, 4-2, and 4-3 respectively.

The levelling of the strapdown INS is provided by the accelerometers which define the local-level plane (pitch, roll). The north orientation is obtained by the gyros which define the alignment orientation (yaw) of the levelled system (see Figure 2-1).

In Table 4-3, a direct comparison is given for yaw (from as built plans) along with the average scaled standard deviations for the attitude quantities.

Table 4-3. Alignment Orientation Results

Run	σ_{pitch} (DMS)	σ_{roll} (DMS)	σ_{yaw} (DMS)	Yaw Error (DMS)
1	0-16-46	0-00-23	21-05-12	-1-58-53
2	0-02-25	0-00-29	23-56-24	37-05-02
3	0-10-33	0-00-18	15-19-00	11-22-22

In most test runs, the absolute accuracy of determining heading of the H778 is about +/- 30°. Bench and laboratory tests have shown much better results in computing yaw to within +/- 5° of the true heading of the system. The large differences and standard deviations for yaw shown here can be attributed to a number of causes. Firstly, the conditions under which these calibration/alignment data sets were collected are typical of most pipeline operating environments. During the static data set collection the system was exposed to thermal changes and vibrations. Secondly, it is not always possible to collect the optimal number of system orientations to estimate the biases and drifts. In the lab results this was possible.

For the results described here, all but the final static set were observed on a concrete floor of a heated (20°C) Pipeline Maintenance (PLM) shop. The last set, which is the final mission alignment set, is observed after the pig is inserted into the pipeline launch facility. The temperatures were -30°C around the trap site. This thermal gradient has a significant effect on the performance of the strapdown INS sensors even though they are temperature compensated.

In addition to the thermal effects, most launch and receive traps on pipelines are collocated with compressor or pump stations. These facilities tend to generate vibration which is sensed by the strapdown unit. As (Britting, 1971) points out, without proper modelling of disturbing effects, accurate alignment is difficult. Vibration at these sites contributed to the alignment error.

These results show the alignment levelling ability of the H778 system. With the exception of run 1 results, the velocity drifts show linear growth due to the misalignment of the system. Run 2 exhibits behavior which may be attributed to movement of the system during the static period. The velocity growth over the 60s period directly reflects the effect of the quantization size and accuracy of the H778 accelerometers. The standard deviations of the attitude parameters provided in Table 4-3 support the position and velocity errors shown. The alignment capability of this system does provide an initial orientation and estimate of the sensor errors but in order to achieve suitable positioning results, velocity aided navigation of the H778 system is required.

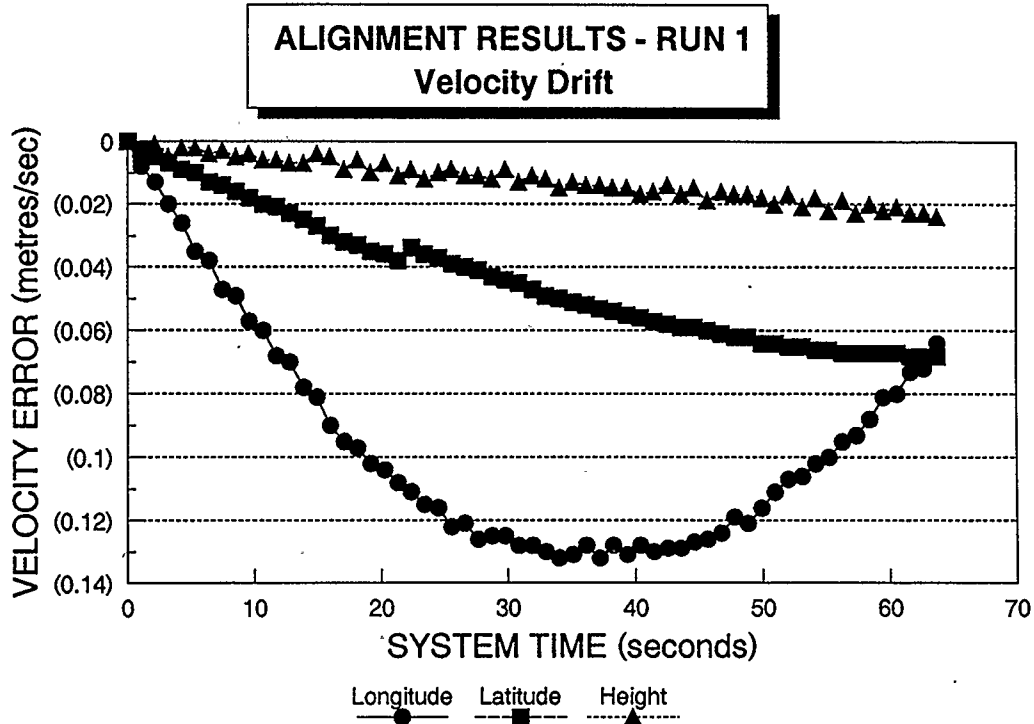


Figure 4-1a. Alignment Velocity Errors - Run 1

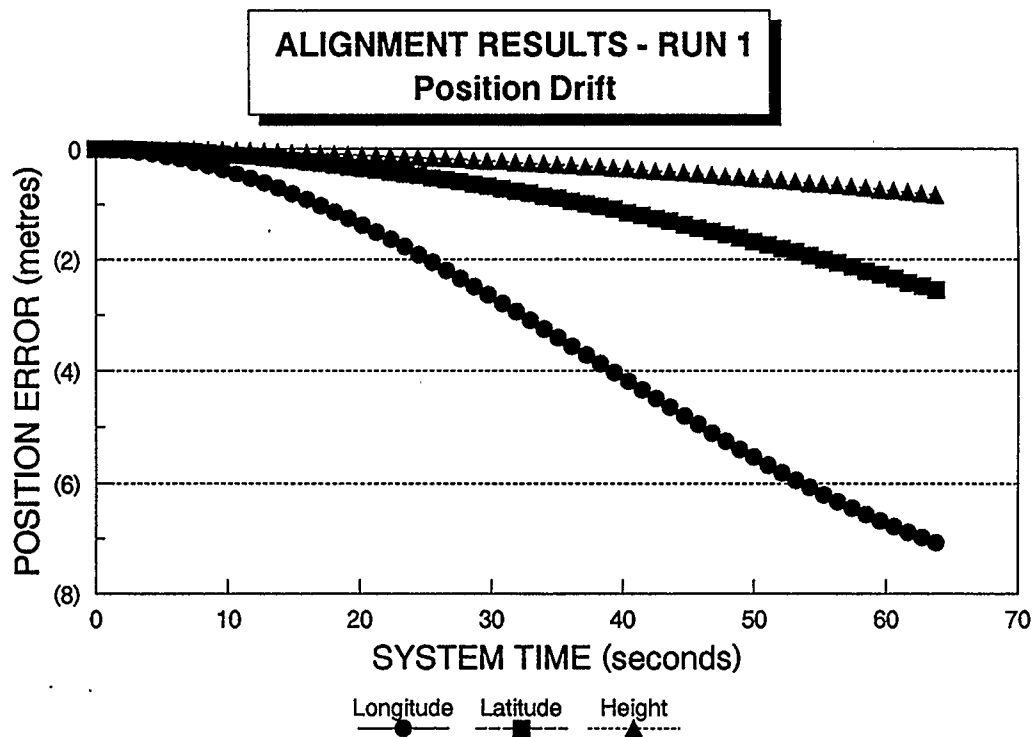


Figure 4-1b. Alignment Position Errors - Run 1

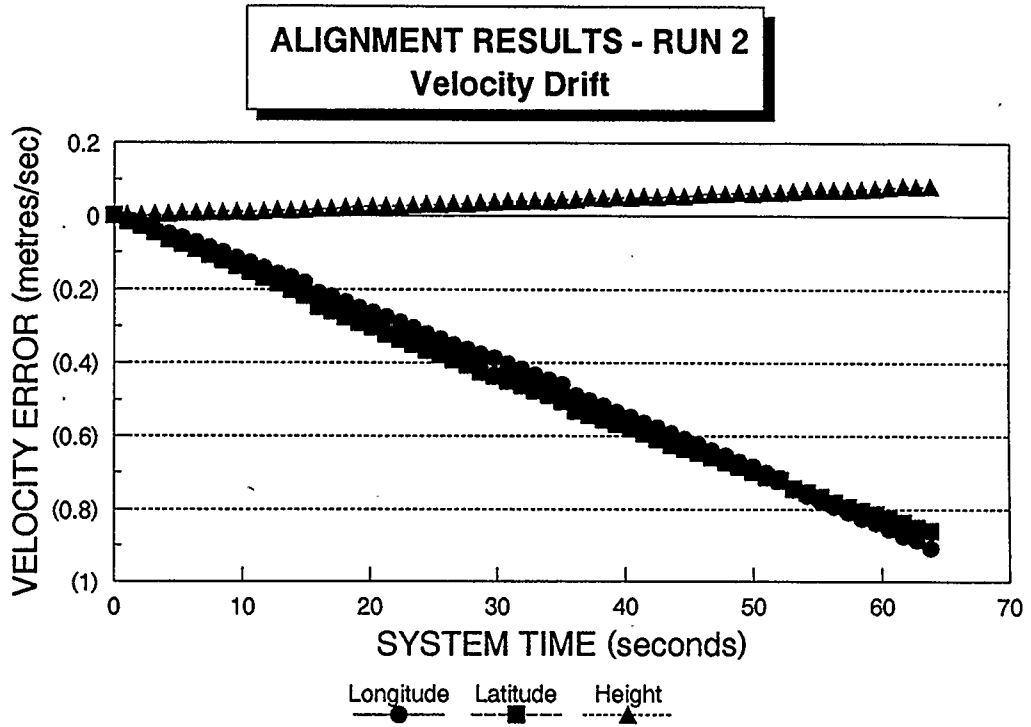


Figure 4-2a. Alignment Velocity Errors - Run 2

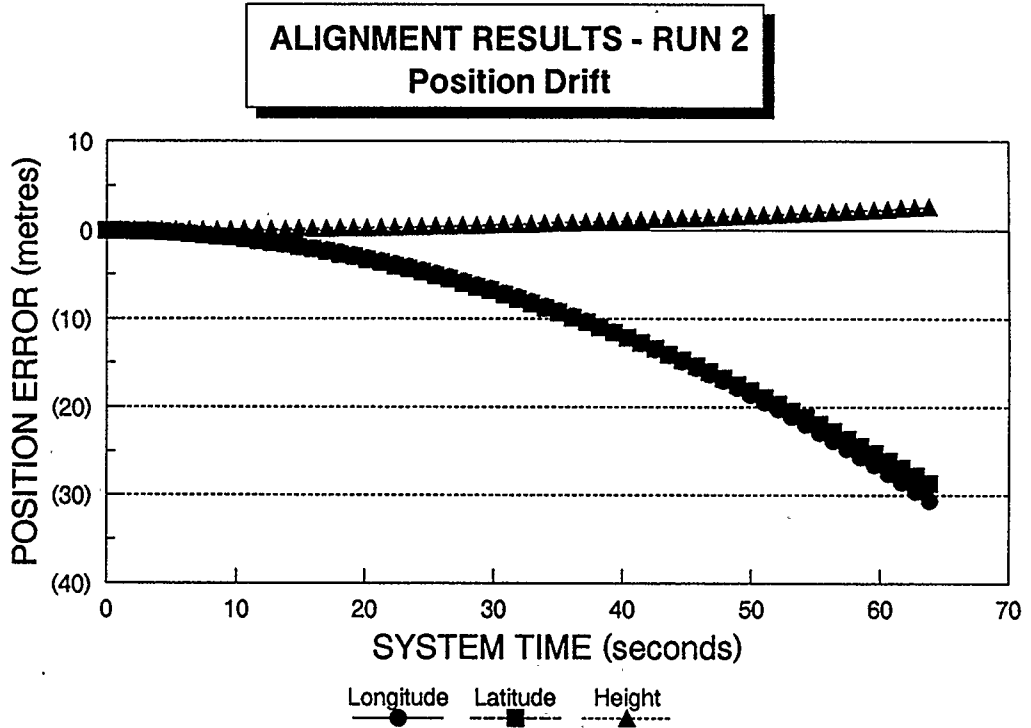


Figure 4-2b. Alignment Position Errors - Run 2

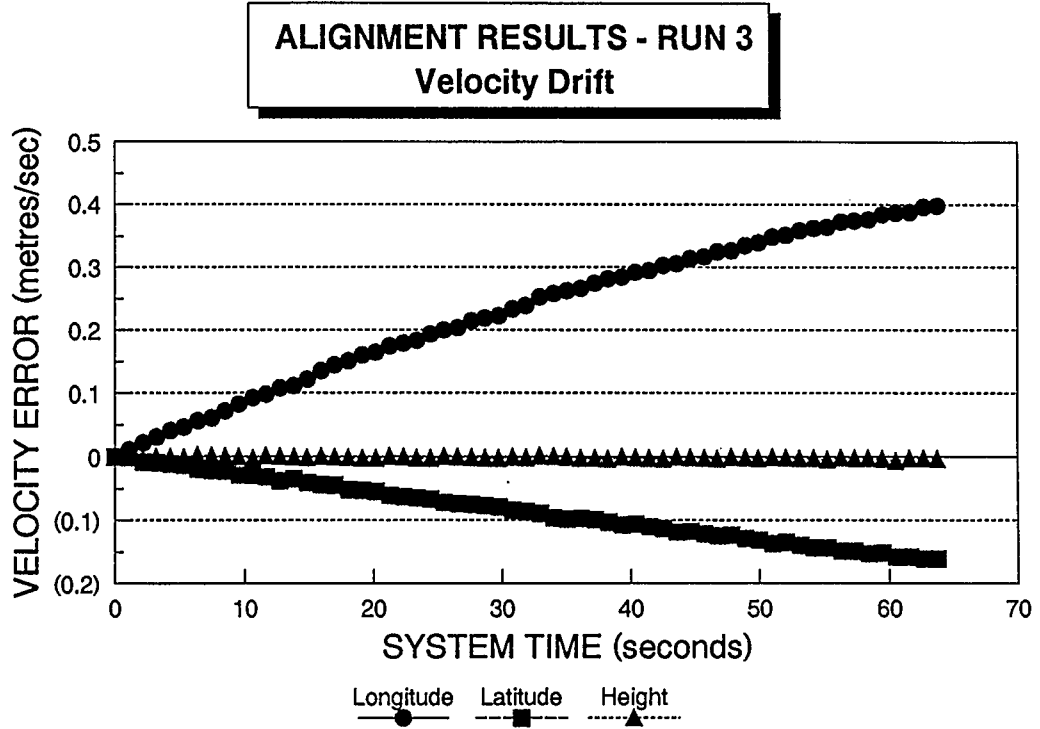


Figure 4-3a. Alignment Velocity Errors - Run 3

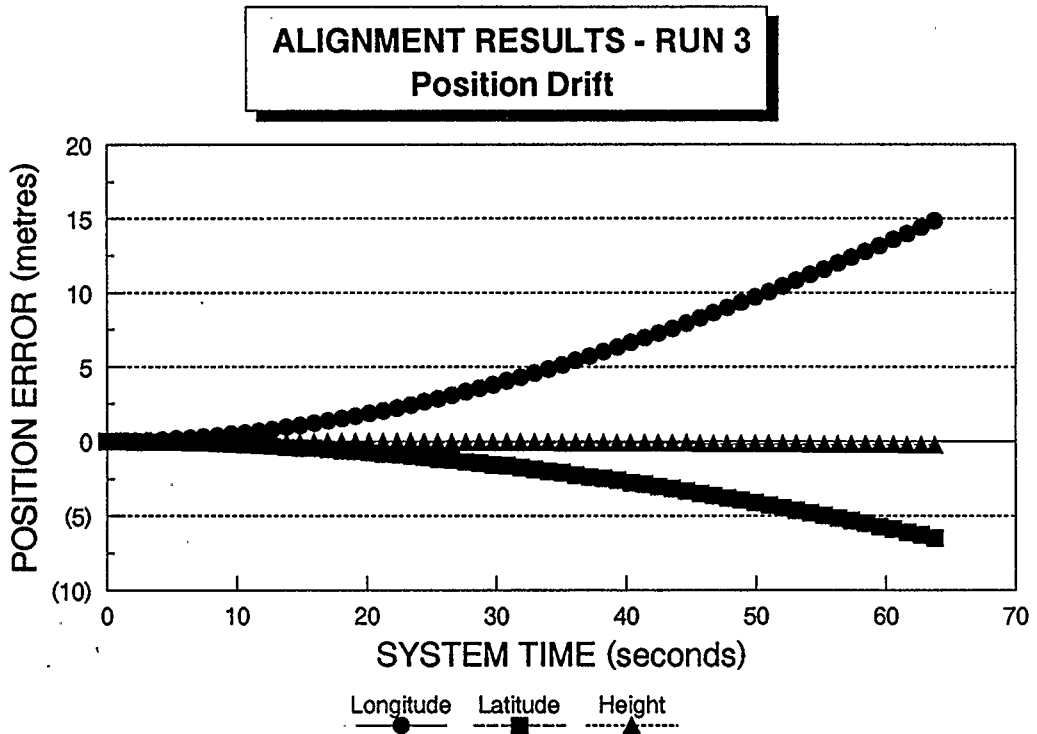


Figure 4-3b. Alignment Position Errors - Run 3

4.1.2 Kalman Filter Parameters

The 15 state Kalman filter uses the velocity information to estimate the state errors of the system and control the time related error growth. The filter is parameterized with initial state variance estimates and spectral density variances. The variances for misorientation, bias, and drift states are set by the results of the coarse alignment adjustment results described in the previous section and denoted by "c-a" in Table 4-4. The remaining states and noise quantities are given initial input values as shown in the Table for the H778.

Table 4-4. Kalman Filter Initialization Parameters

State	σ	spectral density
ε_E	c-a "	1.0 "/s
ε_N	c-a "	1.0 "/s
ε_U	c-a "	10.0 "/s
$\delta\lambda$	0.100 m	0.0 m/s
$\delta\phi$	0.100 m	0.0 m/s
δh	0.100 m	0.0 m/s
$\delta\dot{\lambda}$	0.100 m/s	0.001 m/s/s
$\delta\dot{\phi}$	0.100 m/s	0.001 m/s/s
$\delta\dot{h}$	0.100 m/s	0.001 m/s/s
d_x^b	c-a "/s	0.02 "/s/s
d_y^b	c-a "/s	0.02 "/s/s
d_z^b	c-a "/s	0.02 "/s/s
b_x^b	c-a m/s ²	0.0000012 m/s ² /s
b_y^b	c-a m/s ²	0.0000012 m/s ² /s
b_z^b	c-a m/s ²	0.0000012 m/s ² /s

Correlation times of 10s are used for the Gauss-Markov processes modelling the biases and drifts. This short correlation length was used to allow the sensor error terms to change over a short period of time and assume a large portion of the estimated error distribution from the filter. In effect, these biases and drifts behave as a lumped parameter, estimating the short term sensor errors as well.

The fine alignment phase utilizes the Kalman filter and its initial estimates listed in Table 4-4. The purpose of the fine alignment is to improve the initial estimates from the coarse alignment and improve the navigation results from the system. The stationary data set for the survey mission is processed with the filter run at 1 Hz rates using zero velocity updates and position resets to improve the initial estimates for the error states.

The results of the fine alignment phase for all three runs show slight changes in the pitch and roll attitude, and the drifts and biases. The heading orientation changed significantly, and is not always an improvement to the coarse alignment results as is shown in Table 4-5.

Table 4-5. Fine Alignment Orientation Results

Run	Yaw Error (DMS)
1	-0-24-34
2	8-25-17
3	-6-52-01

4.1.3 Results

The raw inertial output of the strapdown INS is shown in Figure 4-4. The gyro scale is +/- 40 pulse counts which are accumulated over 16 Hz recording frequency. Accelerometer output is +/- 150 pulses, where 128 pulses is the approximate equivalent of normal gravity. From this graph, welds can easily be picked out and the roll dynamics of the system assessed by observing the raw accelerometer output. The method of analyzing horizontal and vertical curvature as described in §3.6 is performed using this raw information. This process is very

useful when immediate curvature analysis is required in the field. As can also be seen from the data, the noise level at these quantization levels of the H778 is very low, and the journey of the pig very smooth.

Figure 4-5 shows the velocity aided navigation results for the first 10km of run 1. The plan view panel on the top is annotated with grid ticks for scale and orientation reference and chainage markers to provide along track distance indication. The profile panel below shows all elevation changes of the pipe as it was laid through creeks, rivers, swamps, etc.. This section of data shows a creek crossing at 500m chainage location. The three orientation angles of pitch, roll, and azimuth follow in the next panels. These quantities show; the creek crossing feature indicated by pitch, the rolling of the pig 4 complete times during this 10km section of pipe, and the heading changes as shown in the plan view panel. This attitude information is the basis for the final computed curvatures. The positioning and curvature accuracy of these results will be presented by comparisons in the next section.

The caliper results provide the ability to map and measure dents and ovality of the pipeline. Estimated residuals are used to indicate the departures of the raw measurements from the circle or ellipse solution. These results are illustrated in Figure 4-6 where a cross-sectional slice of the pipe is shown. A number of successive solutions are superimposed on the display to show the maximum and minimum dimensions of the feature. The solution or ideal pipe shape is shown to reference the scaled residuals describing the measured shape of the pipe. Thus, the size and shape of the anomaly are presented.

The circular model is used in structural assessment and field verification. The original pipe was circular, and this model shows the actual combined ovality, dents, and wrinkle features of the pipe. The ellipse model is used when the effects of ovalization of the pipe are separated from the dent and only the dent itself is reported. The caliper sonar system used on the geometry pig was successfully verified in the field to an accuracy of 1 mm by IPL for 7 test sites on their operating line. These results and numerical analysis capabilities provide accurate and high resolution dent, ovality, and wrinkle mapping of the pipe. When combined with the location from the odometers and position from the strapdown INS, geometric anomalies can be found to within 10m from the nearest detectable feature of the pipeline.

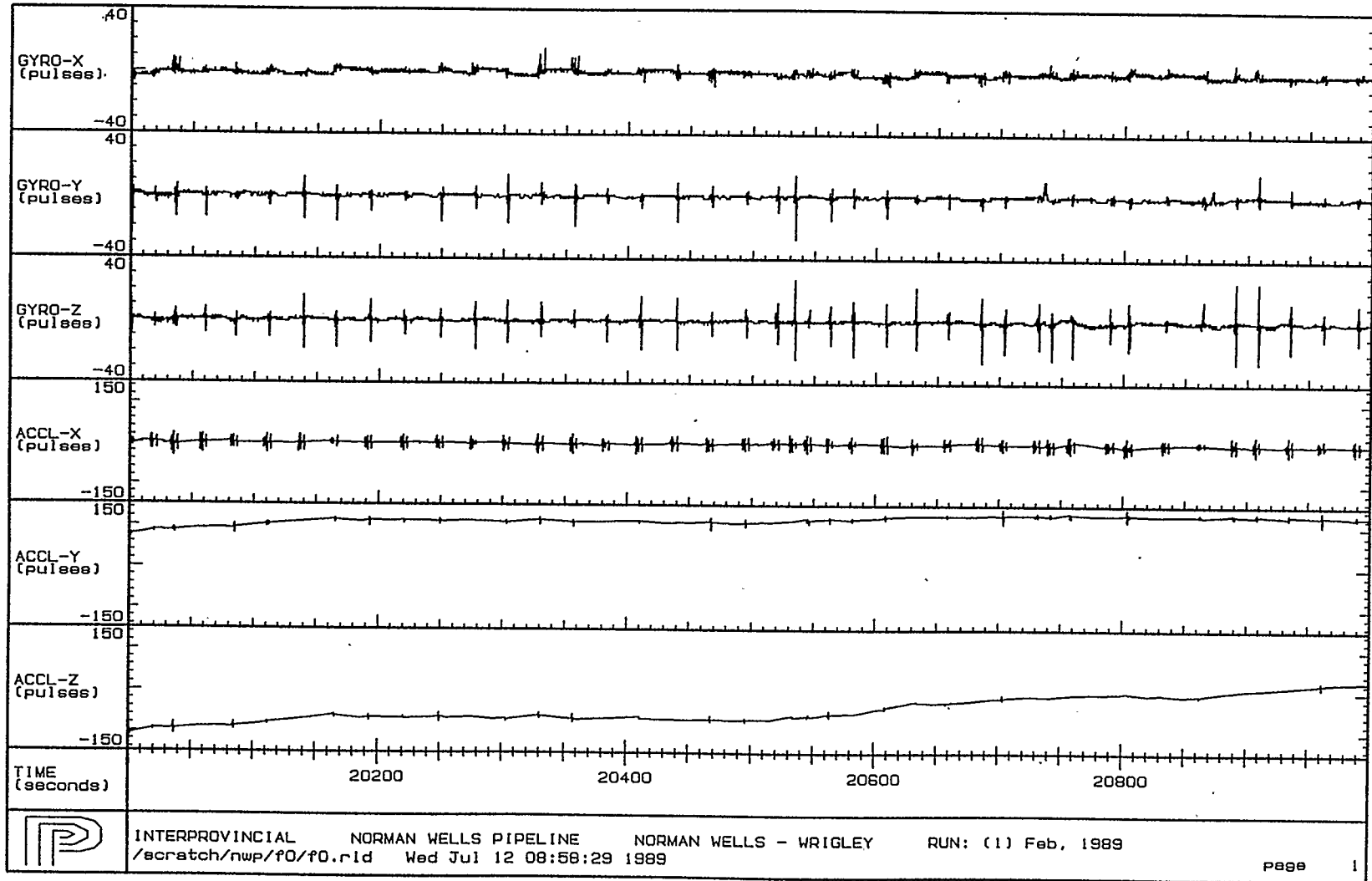


Figure 4-4. Raw H778 Output

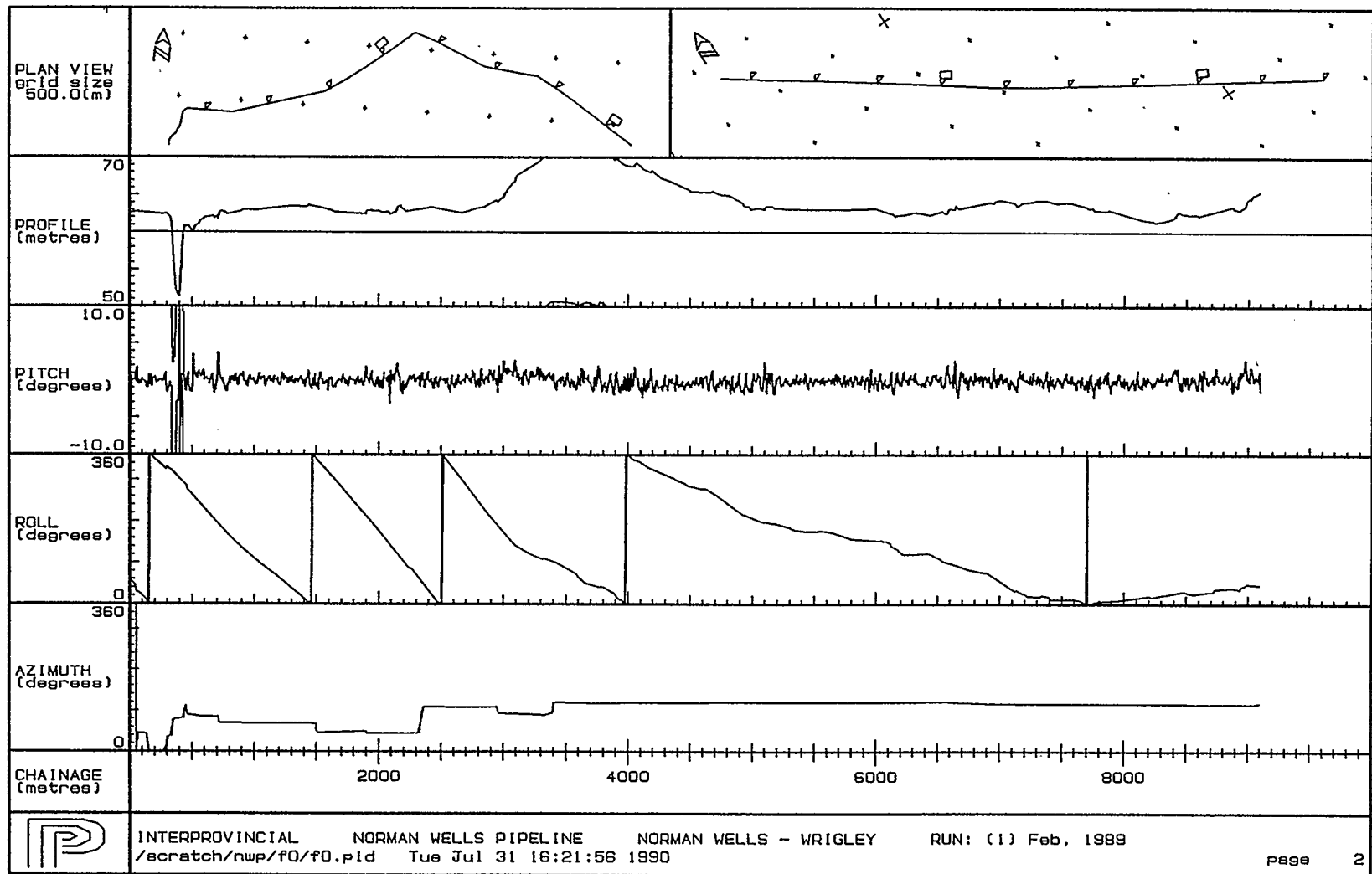


Figure 4-5. Navigation Results

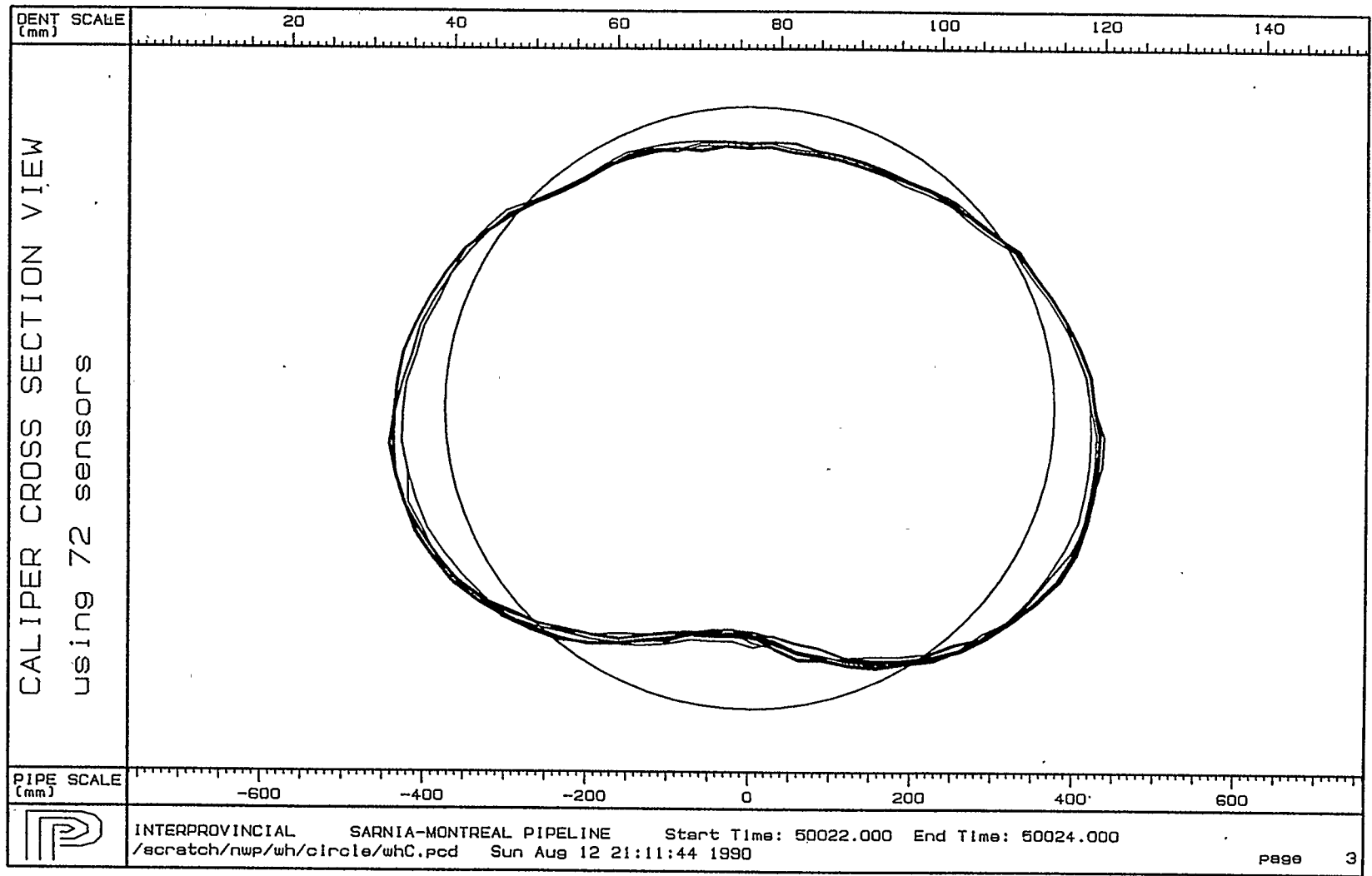


Figure 4-6. Caliper Results

4.2 Multiple Run Deformation Analysis

Deformation analysis is performed by run correlation if a pipeline is inspected at different epochs. The times of different runs are matched using physical features such as welds, bends, valves, or changes from heavy to thin wall sections. Geometric deformation quantities between epochs are computed once the correlation is complete. Comparison of changes of position (local area), curvature, dents, and ovality are possible, for assessing trends and providing prediction. This is advantageous for scheduling and prioritizing any remedial work to be performed on the pipeline based on the current and predicted status of the line.

4.2.1 Results

The position accuracy of the H778 system is made by coordinate comparison. The IPL Norman Wells pipeline database contains UTM (Universal Transverse Mercator) coordinates of the line approximately every 500m or less. In the first 10 Km 26 points were available. The pig navigation data was matched at the start and end of this section by means of a similarity transformation to translate, scale, and rotate the trajectory. This may be construed as a crude smoothing technique to improve the position results.

The results for all three runs are compared by longitude, latitude, and height to the base survey database. The longitude errors shown in Figure 4-7 vary +/- 30m for the 10km section. The heading sensitivity of the results are evident in all three cases by a change in error growth. The latitude errors in Figure 4-8 exhibit a systematic bow in shape. This effect has been shown in other pigging runs to result from drift estimate errors. The height errors shown in Figure 4-9 range +/- 5m along the line are significantly smaller than latitude and longitude errors. This is because height errors resulting from misorientation grow with a cosine function of the misorientation and are therefore small. The profiling capability of the H778 in related river crossing studies up to 2000m in length have shown sub-metre accuracy.

The positioning results shown are largely a function of the quality of the external velocity information provided by the odometers. Data presented here was collected with the initial prototype of the geometry pig which used odometer sensors measuring velocity every 0.30m. In low or changing velocity conditions the instantaneous velocity was not as accurate as that from a near continuous velocity sensing system now employed on the pig. This introduced errors into the velocity observations, but did not effect the accuracy of the along track distance determination. Covariance analysis of the positioning results confirmed these accuracies.

Improvement of the positioning results may be achieved by tuning the Kalman filter parameters listed in Table 4-4. By testing different state variances and noise parameters, the filter is tuned, and a representative set of parameters for the H778 can be determined. The objective is to determine parameters which reflect a particular H778 system. Mission dependant parameters, such as biases, drifts, and heading corrections from sections of the line would further improve the results at the expense of making the processing tedious and time consuming.

Another option to improve the results would be to process the data forward and backward and mean the results. This idea is similar to an optimal smoothing approach. Optimal smoothing is possible, but not feasible due to the large storage requirements for the covariance information. Empirical smoothing of straight sections may be considered as an alternative (Gonthier, 1984).

Azimuth updates and heading constraints may be used if heading or straight section information is available. Position updates can be used and would provide additional improvements for the state estimates and navigation results. However, typical position update information is about 10km apart. Usually not denser than this, therefore little or no improvement can be expected.

An alternative method of navigation is possible by replacing the strapdown INS accelerometer data by odometer output. Using the gyro angular rates and the odometer velocity, accurate local coordinate may be computed.

The position results shown do not reach the 10m accuracy for locating geometric anomalies. But when combined with the odometer information and identification of ground identifiable features such as valves, curves, etc., location to within the required accuracy from the nearest feature is considered feasible.

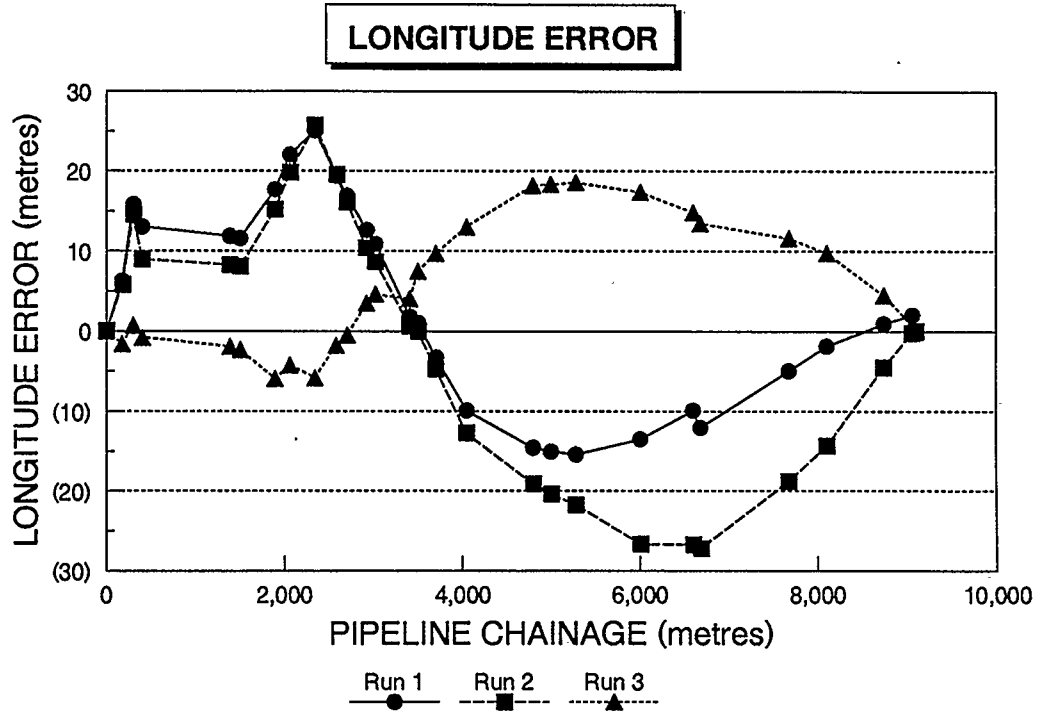


Figure 4-7. Longitude Errors

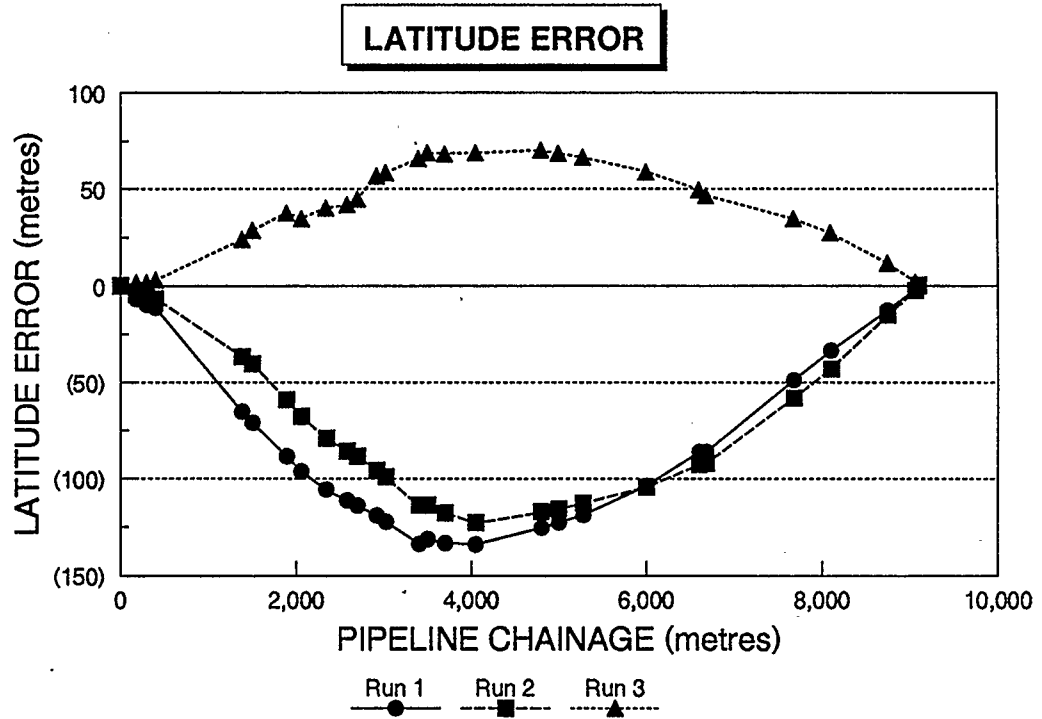


Figure 4-8. Latitude Errors

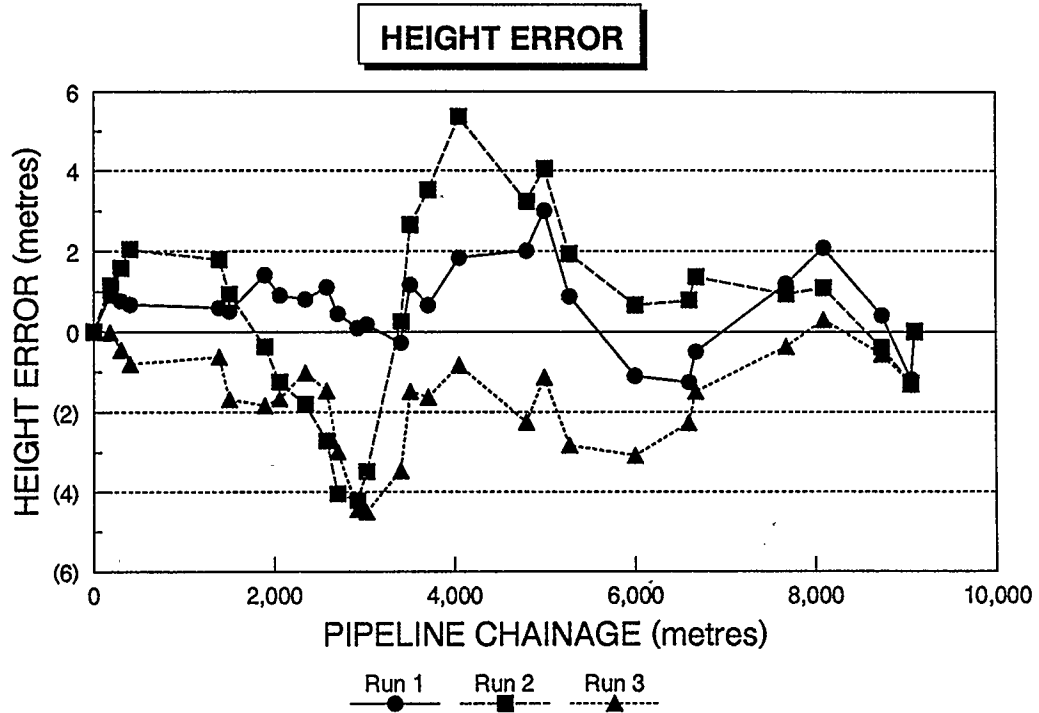


Figure 4-9. Height Errors

Curvature measurement is provided by the gyros of the strapdown INS. These sensors are very accurate in determining attitude change of the moving pig. Shown in Figure 4-10 are a series of vertical field bends produced by a bending machine on site during construction of the pipeline. Positive curvature indicates a sag bend, whereas negative shows an over bend. Figure 4-11 shows a comparison for three runs of this section of the pipe. The mean of the three runs gives essentially the same results shown in Figure 4-10. Differences between the three runs for this section of pipe are shown in Figure 4-11. Note that there is a change of scale between the two figures.

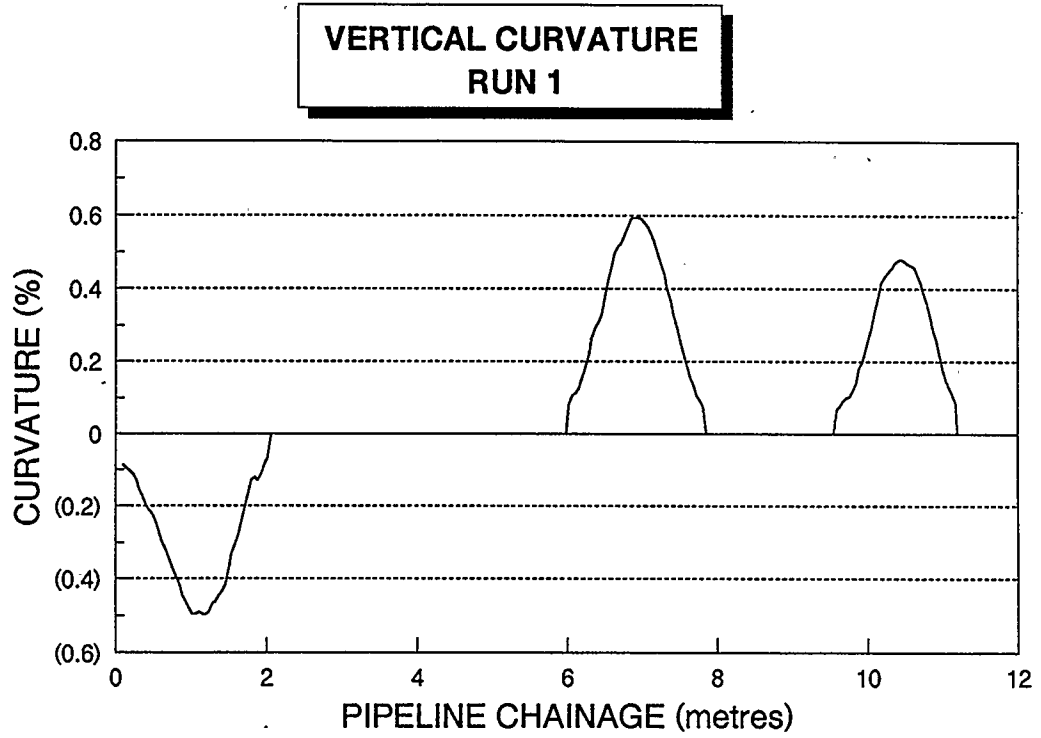


Figure 4-10. Vertical Curvature - Run 1

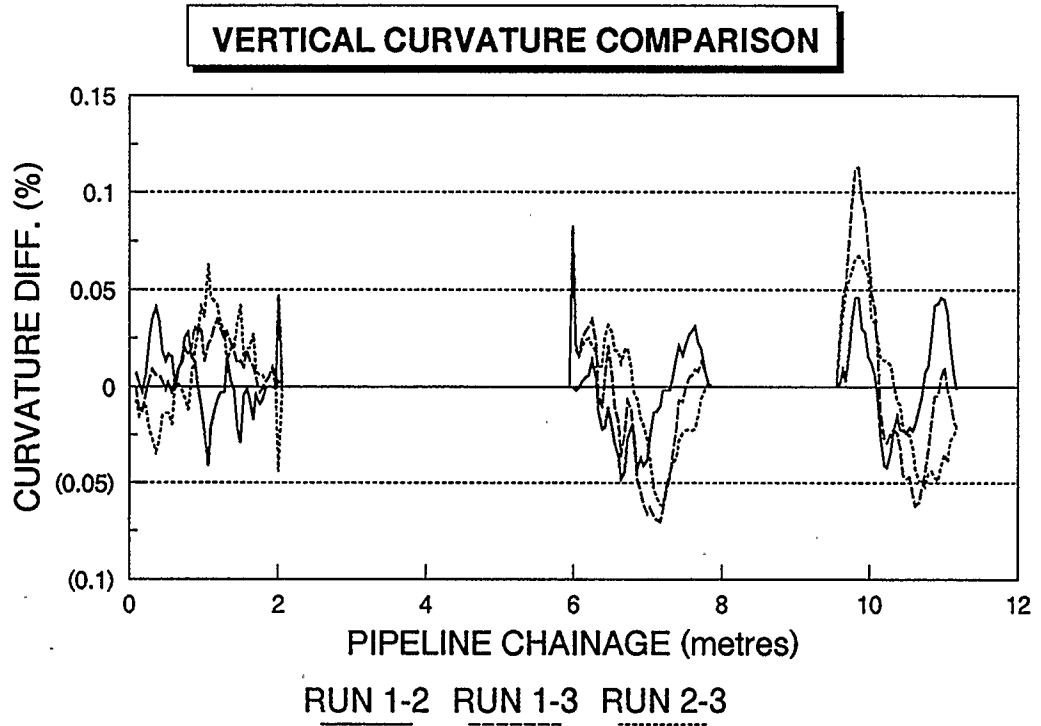


Figure 4-11. Vertical Curvature Comparison

Prescribed bend radii are given and can be checked with the pig, as well as changes in the size and shape of these bends. In the case where originally straight pipe was laid, measured curvature is an accurate indicator of pipe geometry change. The three runs compared were measured over a period of 1 month, during which time no movement of the pipe was expected. The curvature results confirm this to an accuracy of better than 0.1% or $1000\mu\epsilon$ (150m bend radius).

Similar results are shown in Figures 4-12 and 4-13 for horizontal field bends. In addition to measuring field bends, and curvature resulting from pipe movements by external forces, weld misalignments and mitre bends are detected. This information is important when structural analysis is carried out using this data (Pare et al, 1989). This analysis illustrates the accuracy and repeatability of the curvature measurement capabilities of the geometry pig.

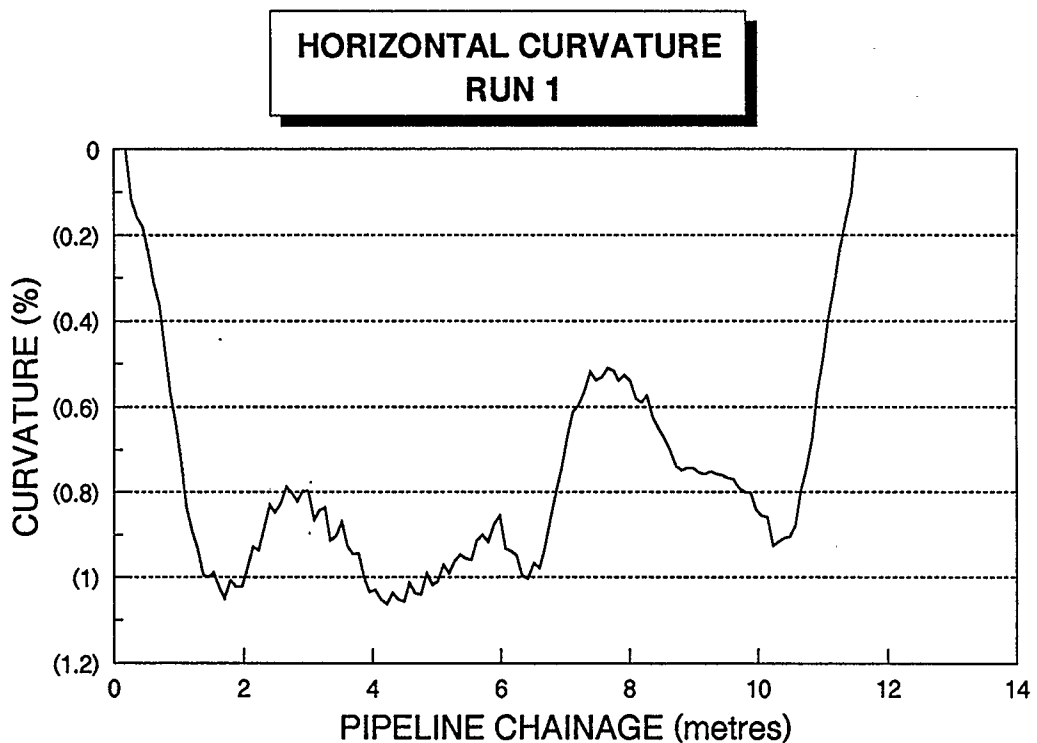


Figure 4-12. Horizontal Curvature - Run 1

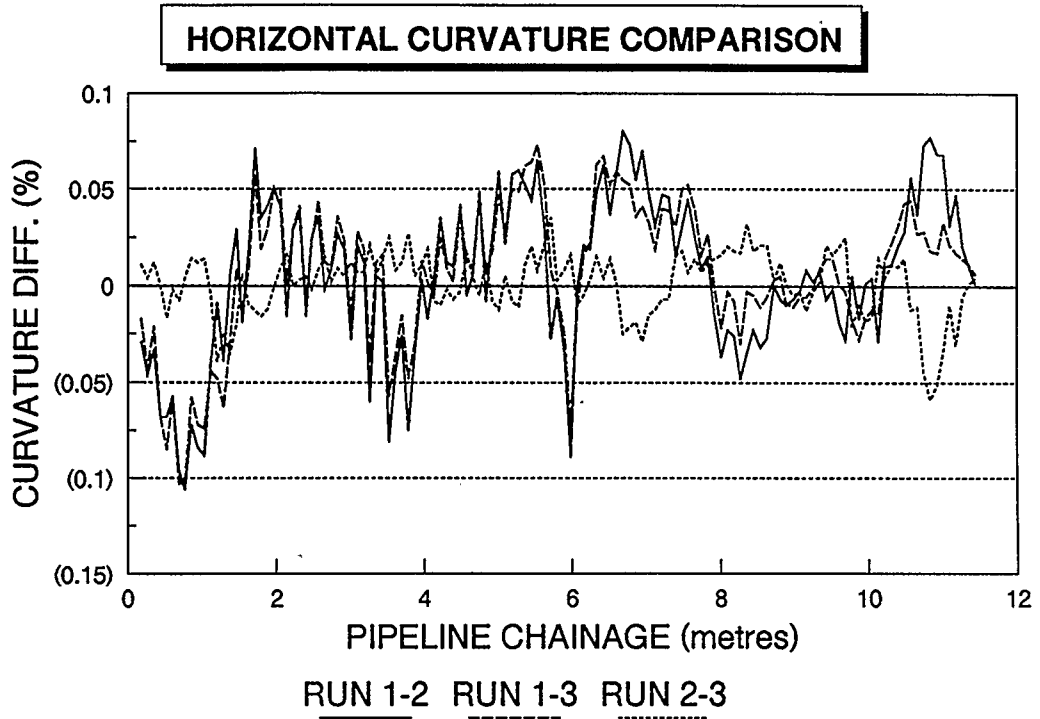


Figure 4-13. Horizontal Curvature Comparison

5 SUMMARY & CONCLUSIONS

Strapdown INS has been successfully used for geometry monitoring of pipelines. This fully integrated system is the first of its kind, which provides accurate measurements of pipeline curvature, dents, ovality, welds and other features, as well as location and position at very high resolution. The end objective is to enhance the safety of operating pipelines.

The advantages of this system over other approaches for geometry monitoring of pipelines are numerous. The system is autonomous, and requires no interaction or operator input during the survey. This is an advantage since most pipelines are buried or inaccessible and are difficult to measure accurately.

Another advantage is that the raw data is recorded digitally, and at high rates to ensure no anomalies are missed. All manipulations, computations, and analysis are done post-mission. This facilitates custom processing, output and display, and high resolution databases for further use in structural analysis.

The system is modular in design. This is an advantage when adapting to service NPS-12 and larger oil or gas pipelines while maintaining the same sensor and measurement approach. Reliability of components and redundancy where possible are features of this integrated system.

A large system of software programs are used for post-mission analysis. A database is constructed for assessing all raw, intermediate, and final results. Using the results for position information and location by chainage, it is expected that geometric anomalies can be located to within 10m relative to the nearest surface identifiable feature along the pipeline. The pipeline operator requires location to this accuracy to carry out maintenance activities.

Curvature radius measurement of 150m and smaller for the complete line monitor the bending of the pipeline which may be caused by thaw induced settlement, frost heave, slope instability, and river crossings. This information is a precise means of assessing geometry change.

Ovality and dent measurement to an accuracy of 1mm, feature location and inventory of valves, and internal diameter changes (wall thickness), is provided by the caliper sonar system. Accurate mapping of these features determines not size but the shape of these features. In the case of dents, the size as well as the gradient of the dent are important parameters in assessing integrity of the line.

Deformations of the pipeline may be detected by comparing data sets from different epochs for the same pipeline. Accurate correlation of the runs is possible using welds and other detected features to compute differences. With numerous runs of a line, prediction or trending of the future status of the line is possible which is useful to the pipeline operator for prioritizing their maintenance activities.

The geometry pig is used for monitoring buried and above ground pipelines as well as offshore pipelines. These lines may transport oil, gas, or even water. In certain applications pressurized air may be the medium.

Pipe movement and geometry changes usually result from external forces. These forces may be produced by; third party equipment encroachment, thaw induced settlement, frost heave, slope instability, and pipe settlement. The geometry pig is used to monitor the resulting changes in shape and location from these causes. The pig can be used for construction and commissioning surveys as well as monitoring of operating lines.

Recommendations to improve the positioning accuracy would be a more accurate velocity sensor system, which at this time has been implemented. Further study and testing of Kalman filter parameters and enhanced processing techniques as suggested in §4.2.1 such as azimuth and position updates and heading constraints would lead to improved results. Empirical smoothing may be incorporated. This improved accuracy may be suitable for generating as built survey data for new as well as old pipelines where no position information is available. Curvature results may be enhanced by applying refined correlation techniques for matching runs, and applying the pig to pipe attitude rectification from the caliper sonars. Another alternative is a more accurate strapdown INS. A system is currently under evaluation which by sensor standards, is an order of magnitude more accurate.

6 BIBLIOGRAPHY

- Adams, J.R., J.W.K. Smith, and A. Pick (1989)
 "In-Situ Pipeline Geometry Monitoring", Proceedings of the Eighth Joint International Conference on Offshore Mechanics and Polar Engineering (OMPE) The Hague, The Netherlands, March, 1989.
- Beer, F.P., and E.R. Johnson Jr. (1976)
 "Mechanics for Engineers, Statics and Dynamics", third edition, McGraw-Hill Publishing Company.
- Britting, K.R. (1971)
 "Inertial Navigation Systems Analysis", Wiley-Interscience.
- Cordell, J.L. (1990)
 "Types of Intelligent Pigs", Pipeline Pigging and Inspection Technology Conference Proceedings, Houston, Texas, February, 1990.
- DMA Technical Report (1987)
 "Supplement to Department of Defense World Geodetic System 1984", Technical Report, Parts I & II, December, 1987.
- Gelb, A. (1974)
 "Applied Optimal Estimation", Massachusetts Institute of Technology, Cambridge, Massachusetts.
- Gonthier, M. (1984)
 "Smoothing Procedures for Inertial Survey Systems of Local Level Type", Publication 20008, Department of Surveying Engineering, The University of Calgary, Calgary, Alberta.
- Honeywell Internal Document (1985)
 "H-778 Functional Description and Operational Data - Inertial Sensor Assembly With Model Differences for the H-778", Honeywell Military Avionics Division, Clearwater Florida.
- Knickmeyer, E.H. (1988)
 "Internal Document", Pulsesearch Consolidated Technology Ltd.
- Krakiwsky, E.J., G. Lachapelle, and K.P. Schwarz (1990)
 "Assessment of Emerging Technologies for Future Navigation Systems in the Canadian Transportation Sector", Published by Research and Development Policy Coordination Transport Canada, July, 1990.
- Martell, H.E., R.V.C. Wong, E.H. Knickmeyer, and K.P. Schwarz (1988)
 "Report on Alignment, Body Axes Transformation and Navigation Equations for a Strapdown Inertial System", Contract Report, Pulsesearch Consolidated Technology Ltd., Calgary, Alberta.

- Nixon, J.F., J. Stuchly, and A.R. Pick (1984)
 "Design of Norman Wells Pipeline for Frost Heave and Thaw Settlement", Offshore Mechanics and Arctic Engineering, (OMAE 84), New Orleans, Louisiana.
- Palmer, A., and T. Jee (1990)
 "Why Pig a Pipeline", Pipeline Pigging and Inspection Technology Conference Proceedings, Houston, Texas, February, 1990.
- Pare, A., T.R. Porter, R.L. Wade, H.A. Anderson, and P.St.J. Price (1989)
 "Optimized Structural Reliability Analysis Using Inertial Pig Data", International Conference on Offshore Mechanics and Polar Engineering (OMPE), The Hague, The Netherlands, March, 1989.
- Porter, T.R., R.L. Wade, and H.A. Anderson (1990a)
 "In-Situ Geometry Pigging: Applications", Pipeline Pigging and Inspection Technology Conference Proceedings, Houston, Texas, February, 1990.
- Porter, T.R., E.H. Knickmeyer, and R.L. Wade (1990b)
 "Pipeline Geometry Pigging: Application of Strapdown INS", Proceedings of the IEEE 1990 PLANS - POSITION, LOCATION AND NAVIGATION SYMPOSIUM, Las Vegas, Nevada, March, 1990.
- Rüeger, J.M. (1982)
 "Inertial Sensors Part I: Gyroscopes", Publication 30002, Department of Surveying Engineering, The University of Calgary, Calgary, Alberta.
- Rüeger, J.M. (1986)
 "Inertial Sensors Part II: Accelerometers", Publication 30008, Department of Surveying Engineering, The University of Calgary, Calgary, Alberta.
- Savage, P.G. (1982)
 "Strapdown Inertial Algorithms", Advances in Strapdown Inertial Systems, AGAARD Lecture Series No. 133.
- Schwarz, K.P., E.H. Knickmeyer, and H.E. Martell (1990)
 "The Use of Strapdown Technology in Surveying", CISM Journal, Vol. 44, No. 1, Spring, 1990.
- Stieler, B., and H. Winter (1982)
 "Gyroscopic Instruments and Their Application to Flight Testing", AGAARD Lecture Series No. 160.
- Vanicek, P., and E.J. Krakiwsky (1982)
 "Geodesy - The Concepts", North-Holland Publishing Company, New York.
- Wei, M., and K.P. Schwarz (1990)
 "A Strapdown Inertial Algorithm Using an Earth-Fixed Cartesian Frame", Navigation - Journal of the Institute of Navigation", Vol.37, No. 2, Summer, 1990.

- Wells, D.E. (1971)
"Matrices", Department of Surveying Engineering, University of New Brunswick,
Fredericton, N.B. Lecture Notes No. 15
- Wertz, J.R. (1978)
"Spacecraft Attitude Determination and Control", D. Reidel Publishing Company Inc.,
Lincoln Building, 160 Old Derby Street, Hingham, Mass. 02043, USA.
- Wong, R.V.C. (1982)
"A Kalman Filter-Smoother for an Inertial Survey System of Local-Level Type",
Publication 20001, Department of Surveying Engineering, The University of Calgary,
Calgary, Alberta.
- Wong, R.V.C. (1988)
"Development of a RLG Strapdown Inertial Survey System", Publication 20027,
Department of Surveying Engineering, The University of Calgary, Calgary, Alberta.